

Nearby early-type galaxies with ionized gas. III

Analysis of line-strength indices with new stellar population models^{*}

F. Annibali^{1,2}, A. Bressan^{2,3,4}, R. Rampazzo³, W. W. Zeilinger⁵ and L. Danese².

¹ STSCI, 3700 San Martin Drive, Baltimore, MD 21218, USA
e-mail: annibali@stsci.edu

² SISSA, Via Beirut 4, 34014 Trieste, Italy

³ INAF - Osservatorio Astronomico di Padova, Vicolo dell'Osservatorio 5, 35122 Padova, Italy

⁴ Instituto Nacional de Astrofísica, Óptica y Electrónica, Apd. Postales 51 y 216, C.P. 72000 Puebla, México

⁵ Institut für Astronomie der Universität Wien, Türkenschanzstraße 17, A-1180 Wien, Austria

Received date; accepted date

ABSTRACT

Aims. The paper is devoted to the study of the underlying stellar population of a sample of 65 nearby early-type galaxies, predominantly located in low density environments, a large fraction of which show emission lines.

Methods. Ages, metallicities, and $[\alpha/\text{Fe}]$ ratios have been derived through the comparison of Lick indices measured at different galacto-centric distances (7 apertures and 4 gradients) with new simple stellar population (SSP) models that account for the presence of α/Fe -enhancement. The SSPs cover a wide range of ages ($10^9 - 16 \times 10^9$ yr), metallicities ($0.0004 \leq Z \leq 0.05$), and $[\alpha/\text{Fe}]$ ratios (0-0.8). To derive the stellar population parameters, we use an algorithm that provides, together with the most likely solution in the (age, Z , $[\alpha/\text{Fe}]$) space, the probability density function along the age-metallicity degeneracy.

Results. We derive a large spread in age, with SSP-equivalent ages ranging from a few to 15 Gyrs. Age does not show any significant trend with central velocity dispersion σ_c , but E galaxies appear on average older than lenticulars. On the contrary, a significant increasing trend of metallicity and $[\alpha/\text{Fe}]$ with σ_c is observed, testifying that the chemical enrichment was more efficient and the duration of the star formation shorter in more massive galaxies. These latter two relations do not depend on galaxy morphological type.

We have also sought possible correlations with the local galaxy density ρ_{xyz} , but neither metallicity nor α -enhancement show clear trends. However, we find that while low density environments (LDE) ($\rho_{xyz} \leq 0.4$) contain very young objects (from 1 Gyr to 4 Gyr), none of the galaxies in the higher density environments (HDE) (40 % of galaxies with a measured density) is younger than 5 Gyrs. Considering the lack of environmental effect on the $[\alpha/\text{Fe}]$ ratio and the high value of $[\alpha/\text{Fe}]$ in some young massive objects, we argue that young galaxies in LDE are more likely due to recent rejuvenation episodes. By comparing the number of “rejuvenated” objects with the total number of galaxies in our sample, and by means of simple two-SSP component models, we estimate that, on average, the rejuvenation episodes do not involve more than 25 % of the total galaxy mass.

The good quality of the data also allow us to analyze the gradients of stellar populations. An average negative metallicity gradient $\Delta \log Z / \Delta \log(r/r_e) \sim -0.21$ is firmly detected, while the age and α -enhancement spatial distributions within $r_e/2$ appear quite flat. These observations suggest that, in a given galaxy, the star formation proceeded on similar timescales all across the central $r_e/2$ region, but with an increasing efficiency toward the center.

Key words. Galaxies: elliptical and lenticular, cD – Galaxies: fundamental parameters – Galaxies: formation – Galaxies: evolution

1. Introduction

This is the third paper of a series dedicated to the study of early-type galaxies with emission lines (Rampazzo et

al. 2005, hereafter Paper I; Annibali et al. 2005, hereafter Paper II). A recent work by Falcón-Barroso et al. (2006) (see also Sarzi et al. 2006) based on SAURON observations shows that the incidence of ionized-gas emission in early-type galaxies is about 75%. By morphological type, lenticular galaxies display a slightly higher content of ionized gas than elliptical galaxies (83% versus 66%), in good agreement with the pioneering survey performed

Send offprint requests to: F. Annibali

* Tables 5-7 and 9-12 are only available in electronic form at the CDS via anonymous ftp to cdsarc.u-strasbg.fr (130.79.128.5) or via <http://cdsweb.u-strasbg.fr/cgi-bin/qcat?J/A+A/>

by Macchietto et al. (1996), who found emission in 85% of the lenticulars and 68% of the ellipticals in their sample. Falcón-Barroso et al. (2006) found similar percentages when their sample was divided according to environment (83% field, 66% cluster). Furthermore, the incidence of ionized gas shows no correlation with either luminosity or the presence of a bar in the galaxy. The above percentages suggest that the phenomenon of emission lines is quite common among early-type galaxies: early-type galaxies without emission lines are more exceptions rather than the rule in this class of galaxies. The first step to understanding the evolution of these galaxies and the nature of their ionized gas consists in studying the galaxy underlying stellar population.

For this purpose we make use of the absorption-line indices that have been proven to be a powerful tool to disentangle age and metallicity effects (e.g., Buzzoni et al. 1992; Worthey 1992; González 1993 (G93); Worthey 1994; Buzzoni et al. 1994; Worthey et al. 1994; Bressan et al. 1996; Leonardi & Rose 1996; Worthey & Ottaviani 1997; Trager et al. 1998; Longhetti et al. 1998; Vazdekis 1999; Longhetti et al. 1999; Longhetti et al. 2000; Trager et al. 2000a; Kuntschner 2000; Beuing et al. 2002; Kuntschner et al. 2002; Mehlert et al. 2003). More recently the interpretation has been faced with the more difficult task of also accounting for the presence of non-solar scaled abundance patterns in early-type galaxies, and of deriving age, metallicity, and $[\alpha/\text{Fe}]$ ratio at the same time (e.g., Tantalo et al. 1996; Tantalo & Chiosi 2004a; Thomas et al. 2003; Thomas et al. 2005). Indeed, it has been shown that the α/Fe element ratio plays a fundamental role in deriving the formation epochs. This ratio, in fact, quantifying the relative importance of Type II and Type Ia supernovae in the enrichment of the ISM, carries information about the timescale over which the star formation occurred (Greggio & Renzini 1983; Matteucci & Greggio 1986; Pagel & Tautvaisiene 1995; Thomas et al. 1998).

In this paper we try to constrain the epoch of the baryon assembly of our sample of 65 nearby early-type galaxies predominantly located in low density environments, a large fraction of which show emission lines (Paper I and II), and seek possible correlations with their morphological type (elliptical and lenticular), velocity dispersion, and environmental density. A large part of this paper is dedicated to the development of our own α -enhanced models and to the comparison with the models already presented in the literature. The stellar population parameters are derived by means of a new algorithm based on the probability density function. The algorithm provides, together with the most probable solution in the (age, Z , $[\alpha/\text{Fe}]$) space, the solutions along the age-metallicity degeneracy that are within 1σ error from the observed index values. Our analysis is based on the use of three different line-strength index diagnostics, including the Mgb index, the $\langle\text{Fe}\rangle$ index, and a Balmer line ($\text{H}\beta$, $\text{H}\gamma$, or $\text{H}\delta$). The use of higher order Balmer lines allows us to minimize spurious effects that may arise from uncertainties in the emission correction of the $\text{H}\beta$ absorption line. The pa-

per is organized as follows. Section 2 presents an overview of the sample, summarizing its main properties and focusing on the delicate step of the correction for emission infilling of the most commonly used age indicator, the $\text{H}\beta$ absorption line. In Sect. 3 a complete description of the procedure adopted to compute the new α -enhanced SSPs is provided. Section 4 describes how the new SSP models have been implemented within an algorithm that allows us to derive the stellar population parameters, i.e., age, metallicity, and α/Fe ratio. Section 5 presents the results. In particular we analyze both the stellar population parameters derived for the apertures and gradients, and their relations with velocity dispersion and local galaxy density. In Sect. 6 we discuss our results and compare them with the literature. Finally, a summary and our conclusions are presented in Sect. 7.

2. Further analysis of the line-strength indices data set

2.1. A sample overview

The procedure of data reduction and analysis of the 65 nearby early-type galaxies studied here has been already discussed in Papers I and II. Table 1 summarizes the main characteristics of the sample. Column (1) gives the galaxy identification name; Col. (2) and (3) provide the galaxy morphological classification according to RSA (Sandage & Tamman 1987) and RC3 (de Vaucouleurs et al. 1991), respectively: only in few cases do the two catalogues disagree in the distinction between E and S0 classes; Col. (4) gives the galaxy systemic velocity, V_{hel} , which is lower than $\sim 5000 \text{ km s}^{-1}$; Col. (5) provides the richness parameter ρ_{xyz} (Tully 1988): it represents the density of galaxies brighter than -16 apparent B-mag in the vicinity of the entry, in galaxies $\times \text{Mpc}^{-3}$. The local density was determined on a three-dimensional grid with 0.5 Mpc spacings. A Gaussian smoothing function was used to calculate the contribution of each member of the sample brighter than -16 B-mag to the density of the specific location. In the Tully catalogue, the galaxies (considered in the local environment) within 40 Mpc (3000 km s^{-1}) with an apparent magnitude B-mag ≤ -16 are 2189. If one entry is at a distance larger than 40 Mpc, the local density is not recorded. The galaxies of our sample are mainly located in low density environments. The local density of our galaxies varies from $\rho_{xyz} \approx 0.1$, characteristic of very isolated galaxies, to $\rho_{xyz} \approx 4$, which is characteristic of denser galaxy regions in the Virgo cluster. For comparison, in the Tully 1988 catalogue, objects like NGC 1399 and NGC 1389, Fornax cluster members, have values of $\rho_{xyz} = 1.59$ and 1.50, respectively. Thus, our sample, even though biased towards low density environments, contains a fraction of galaxies in relatively dense environments.

The sample spans a large range in central velocity dispersion, \approx from 115 to 340 km s^{-1} (see Papers I and II for detailed descriptions). Our long-slit spectra cover the (3700 - 7250) Å wavelength range with a spectral resolu-

tion of ≈ 7.6 Å at 5550 Å. For the detailed description of the data reduction procedure and of the derivation of line-strength indices in the Lick system, we refer to Papers I and II. We only recall here that for each galaxy, 25 Lick indices (21 belonging to the original Lick set (see Trager et al. (1998) for the pass-band definitions) plus 4 higher order Balmer lines introduced by Worthey & Ottaviani (1997)) have been measured for 7 luminosity weighted apertures (with radii: 1.5'', 2.5'', 10'', $r_e/10$, $r_e/8$, $r_e/4$, and $r_e/2$), corrected for the galaxy ellipticity, and 4 gradients ($0 \leq r \leq r_e/16$, $r_e/16 \leq r \leq r_e/8$, $r_e/8 \leq r \leq r_e/4$, and $r_e/4 \leq r \leq r_e/2$).

2.2. $H\beta$ correction for emission infilling

Because of the presence of emission in a significant fraction of the sample, the problem of possible contamination of the $H\beta$ absorption line deserves particular attention. In Papers I and II we have shown two different methods to correct the $H\beta$ index for possible emission infilling, based respectively on the measure of the $[OIII]\lambda 5007$ Å and of the $H\alpha$ emission lines. The first method is based on the correlation found by G93 between the $H\beta$ and the $[OIII]$ emission in his sample of early-type galaxies, such that $EW(H\beta_{em})/EW([OIII]\lambda 5007) = 0.7$. The second method rests on the possibility of measuring the $H\alpha$ emission at 6563 Å, from which the emitted flux in the $H\beta$ line results in $F_{H\beta} = 1/2.86 F_{H\alpha}$ (Osterbrock 1989). In Paper I and II, we have shown that the corrections derived from the two different methods are statistically similar. We then provided the final $H\beta$ indices, applying the correction from the $[OIII]\lambda 5007$. We noticed, however, that the scatter of the relation derived by G93 is large, and that small variations in the $H\beta$ index correspond to large differences in the derived stellar population parameters when compared with models.

A comparison of the emission corrections derived from the $[OIII]\lambda 5007$ and $H\alpha$ lines, respectively, is also performed by Denicoló et al. (2005a) for their sample of early-type galaxies. The authors show that the differences in the emission corrections derived through the two methods are small for the majority of galaxies, but argue that it is very dangerous to rely on the use of the $[OIII]\lambda 5007$ alone because the $[OIII]\lambda 5007/H\beta$ ratio may be very different from galaxy to galaxy. They use the $H\alpha$ to correct the $H\beta$ index.

The uncertainties concerning the emission corrections derived from the $H\alpha$ line mainly rest on the assumption of a value for the $H\alpha$ in absorption. Denicoló et al. (2005a) adopt an absorption value on the basis of the $H\alpha$ EW measured for their sample of stars (mainly K). Differently, as described in Papers I and II, we computed the emitted flux in the $H\alpha$ line using, as a reference, the spectrum of an elliptical galaxy (NGC1426) lacking emission lines or dust. This galaxy is located in the low tail of the $Mg2-\sigma$ relation. However, we verified that the use of a giant elliptical reflects in a difference of 0.03 Å in the value of the

Table 1 Sample overview

Ident	RSA	RC3	V_{hel} km s ⁻¹	ρ_{xyz} Gal. Mpc ⁻³
NGC 128	S02(8) pec	S0 pec sp	4227	
NGC 777	E1	E1	5040	
NGC 1052	E3/S0	E4	1475	0.49
NGC 1209	E6	E6:	2619	0.13
NGC 1297	S02/3(0)	SAB pec:	1550	0.71
NGC 1366	E7/S01(7)		1310	0.16
NGC 1380	S03(7)/Sa	SA0	1844	1.54
NGC 1389	S01(5)/SB01	SAB(s)0:-	986	1.50
NGC 1407	E0/S01(0)	E0	1766	0.42
NGC 1426	E4	E4	1443	0.66
NGC 1453	E0	E2	3906	
NGC 1521	E3	E3	4165	
NGC 1533	SB02(2)/SBa	SB0-	773	0.89
NGC 1553	S01/2(5)pec	SA(r)0	1280	0.97
NGC 1947	S03(0) pec	S0- pec	1100	0.24
NGC 2749	E3	E3	4180	
NGC 2911	S0p or S03(2)	SA(s)0: pec	3131	
NGC 2962	RSB02/Sa	RSAB(rs)0+	2117	0.15
NGC 2974	E4	E4	1890	0.26
NGC 3136	E4	E:	1731	0.11
NGC 3258	E1	E1	2778	0.72
NGC 3268	E2	E2	2818	0.69
NGC 3489	S03/Sa	SAB(rs)+	693	0.39
NGC 3557	E3		3038	0.28
NGC 3607	S03(3)	SA(s)0:	934	0.34
NGC 3818	E5	E5	1701	0.20
NGC 3962	E1	E1	1822	0.32
NGC 4374	E1	E1	1060	3.99
NGC 4552	S01(0)	E	322	2.97
NGC 4636	E0/S01(6)	E0-1	937	1.33
NGC 4696	(E3)	E+1 pec	2958	0.00
NGC 4697	E6	E6	1241	0.60
NGC 5011	E2	E1-2	3104	0.27
NGC 5044	E0	E0	2704	0.38
NGC 5077	S01/2(4)	E3+	2764	0.23
NGC 5090	E2	E2	3421	
NGC 5193	S01(0)	E pec	3711	
NGC 5266	S03(5) pec	SA0:-	3074	0.35
NGC 5328	E4	E1:	4671	
NGC 5363	[S03(5)]	IO:	1138	0.28
NGC 5638	E1	E1	1676	0.79
NGC 5812	E0	E0	1930	0.19
NGC 5813	E1	E1-2	1972	0.88
NGC 5831	E4	E3	1656	0.83
NGC 5846	S01(0)	E0+	1709	0.84
NGC 5898	S02/3(0)	E0	2267	0.23
NGC 6721	E1	E+:	4416	
NGC 6758	E2 (merger)	E+:	3404	
NGC 6776	E1 pec	E+pec	5480	
NGC 6868	E3/S02/3(3)	E2	2854	0.47
NGC 6875	S0/a(merger)	SAB(s)0- pec:	3121	
NGC 6876	E3		3836	
NGC 6958	R?S01(3)	E+	2652	0.12
NGC 7007	S02/3/a	SA0:-	2954	0.14
NGC 7079	SBa	SB(s)0	2670	0.19
NGC 7097	E4	E5	2404	0.26
NGC 7135	S01 pec	SA0- pec	2718	0.32
NGC 7192	S02(0)	E+:	2904	0.28
NGC 7332	S02/3(8)	S0 pec sp	1207	0.12
NGC 7377	S02/3/Sa pec	SA(s)0+	3291	
IC 1459	E4	E	1659	0.28
IC 2006	E1	E	1350	0.12
IC 3370	E2 pec	E2+	2934	0.20
IC 4296	E0	E	3762	
IC 5063	S03(3)pec/Sa	SA(s)0+:	3402	

computed $H\beta$ emission. Denicoló et al. (2005a) allowed for a reasonable range of $H\alpha$ absorption strengths and determined that the difference in the emission correction is smaller than 0.1 Å. In this paper we adopt the direct estimate derived from the $H\alpha$ emission line for the correction of the $H\beta$ index. The adopted $H\beta$ values can be easily recovered from Papers I and II, where we provided, together with the final indices in the Lick system, the $H\beta$ emission estimates derived both from the $[OIII]\lambda 5007$ and $H\alpha$ lines.

3. Modelling line-strength indices for simple stellar populations

3.1. Standard models

Following the procedure described in Bressan et al. (1996), to which we refer for details, we have derived line-strength indices for SSPs. Indices are constructed by means of a central band-pass and two pseudo-continuum band-passes on either side of the central band. Molecular bands are expressed in magnitude, while atomic features are expressed in equivalent width (EW). The definition in EW is:

$$I_{EW} = (1 - F_R/F_C) \Delta\lambda, \quad (1)$$

while the definition in magnitude is

$$I_{mag} = -2.5 \log (F_R/F_C), \quad (2)$$

where F_R and F_C are the fluxes in the line and in the pseudo-continuum, respectively, and $\Delta\lambda$ is the width of the central band. The flux F_C is obtained by interpolating the fluxes in the blue and red pseudo-continua bracketing the line of interest to the central wavelength of the absorption band. We used the passband definitions provided in Trager et al. (1998) for the original 21 Lick indices, and in Worthey & Ottaviani (1997) for the higher-order Balmer lines. The integrated indices for SSPs are based on the Padova library of stellar models (Bressan et al. 1994) and accompanying isochrones (Bertelli et al. 1994). The SSPs indices are calculated using the following method. We derive both the pseudo-continuum flux F_C from the library of stellar spectra used by Bressan et al. (1994) and implemented by the revision of Tantalo et al. (1996), and the line strength index I_{EW} or I_{mag} from the fitting functions (FFs) of Worthey et al. (1994) and Worthey & Ottaviani (1997), for each elementary bin $\Delta \log \frac{L}{L_\odot}$ and $\Delta \log T_{eff}$ of a given isochrone in the HR diagram. The residual flux in the central feature F_R is recovered from F_C and I_{EW} (I_{mag}) by inverting Eqs. (1) and (2). For an SSP of age T and metallicity Z, the fluxes in the line and in the continuum, $F_{R,SSP}(T, Z)$ and $F_{C,SSP}(T, Z)$, are then obtained by integrating F_C and F_R along the isochrone:

$$F_{k,SSP}(T, Z) = \int_{M_L}^{M_U} \phi(M) F_k(M, T, Z) dM, \quad (3)$$

where k denotes the flux in the continuum (C) or in the line (R), $\phi(M)$ is the Initial Mass Function (IMF) defined between M_L and M_U , and $F_k(M, T, Z)$ is the flux for a star of mass M , age T , and metallicity Z . Once the integrated fluxes, $F_{R,SSP}$ and $F_{C,SSP}$, are computed, the index definition (Eqs. (1) and (2)) is applied to get the integrated SSP index back. Our SSP models have been computed adopting a Salpeter (1955) IMF slope between 0.15 and $120 M_\odot$.

3.2. α /Fe-enhanced models

To compute the SSP models presented in Sect. 3.1, we have adopted stellar isochrones based on solar-scaled abundances and FFs calibrated on Milky Way stars. For these reasons the standard SSPs reflect the solar element abundance pattern. However, there are several evidences for supersolar $[\alpha/Fe]$ ratios in early-type galaxies (Peletier 1989; Worthey et al. 1992; Davies et al. 1993; Carollo & Danziger 1994; Bender & Paquet 1995; Fisher et al. 1995; Mehrt et al. 1998; Jørgensen 1999; Kuntschner 2000; Longhetti et al. 2000 and others).

The major effect of non-solar abundance patterns is on the stellar atmospheres. For a given effective temperature, gravity, and total metallicity, the stellar spectrum, and thus the line-strength indices that are measured in it, depend on the specific ratios between the element abundances. To account for this effect, we apply a correction to the index derived from the FFs using tabulated index responses to element abundance variations. The responses are derived from model atmospheres and synthetic spectra (Tripicco & Bell 1995 (hereafter TB95); Korn et al. 2005 (hereafter K05), Munari et al. 2005 (hereafter Mu05)). A second, less important effect is on the evolution of the star and on the stellar opacities. A fully self-consistent α -enhanced SSP model should in principle use α /Fe-enhanced stellar evolutionary tracks (Weiss et al. 1995; Salaris & Weiss 1998; Van den Berg et al. 2000; Salasnich et al. 2000). In the literature, several α -enhanced SSP models have been presented. In all models a correction is applied to the index value to account for the impact of the α /Fe-enhancement on the stellar atmosphere (Weiss et al. 1995; Tantalo, Chiosi & Bressan 1998; Trager et al. 2000a, Thomas et al. 2003 (hereafter TMB03), Thomas et al. 2004; Tantalo & Chiosi 2004b; Tantalo et al. 2004; Korn et al. 2005). SSPs adopting α /Fe-enhanced stellar evolutionary tracks have been produced as well (Thomas & Maraston 2003; Tantalo & Chiosi 2004a), but current enhanced models seem to overestimate the blueing of the stellar evolutionary tracks. In this section we present new SSP models that are based on solar-scaled isochrones (Bertelli et al. 1994) and where only the direct effect of the enhancement on the stellar atmosphere is taken into account. The models are available to the public at <http://www.inaoep.mx/~abressan> or www.stsci.edu/~annibali/.

3.3. α -enhanced chemical compositions

Following the procedure adopted by TMB03, we assign elements to three groups: the *enhanced* group (α -elements), the *depressed* group (Fe-peak elements), and the *fixed* group (elements left unchanged). Taking as a reference model a mixture of total metallicity Z and solar partitions, a new mixture with the same global metallicity Z , but with supersolar $[\alpha/Fe]$ ratio is produced by increasing the abundance of the α -group and decreasing that of

the Fe-group in such a way that the two mass fraction variations balance.

If $X_{\alpha,\odot}$ and $X_{Fe,\odot}$ are the total mass fractions of the two groups for the solar mixture, and X_α and X_{Fe} are the mass fractions in the new mixture, the degree of enhancement is expressed by the quantity

$$[\alpha/Fe] = \log \frac{X_\alpha}{X_{Fe}} - \log \frac{X_{\alpha,\odot}}{X_{Fe,\odot}}. \quad (4)$$

The quantities $X_{\alpha,\odot}$ and $X_{Fe,\odot}$ are computed by summing up the mass fractions of the elements within the α and Fe groups in the solar-scaled mixture, and thus depend on how elements are allocated within the groups.

For an arbitrary mixture, the i -th element mass fraction is:

$$X_i = f_i \frac{Z}{Z_\odot} X_{i,\odot}, \quad (5)$$

where $f_i = 1$ for solar-scaled abundances, $f_i > 1$ if the element is enhanced with respect to the solar-scaled composition, and $f_i < 1$ if the element is depressed. Once the element allocation within the three groups and the global enhancement $[\alpha/Fe]$ has been defined, we derive the quantities f_i . Since in our assumption all the elements within a group are enhanced/depressed by the same amount, it is sufficient to compute f_α and f_{Fe} .

Let us call Z_b and $[\alpha/Fe]_b$ the total metallicity and the enhancement of the starting base model, and Z_n and $[\alpha/Fe]_n$ the same quantities in the new mixture. The enhanced, depressed, and fixed group mass fractions in the new mixture (n) are related to the base model (b) quantities according to:

$$\begin{aligned} X_{\alpha,n} &= f_\alpha \frac{Z_n}{Z_b} X_{\alpha,b}, \\ X_{Fe,n} &= f_{Fe} \frac{Z_n}{Z_b} X_{Fe,b}, \\ X_{0,n} &= \frac{Z_n}{Z_b} X_{0,b} \end{aligned} \quad (6)$$

The quantities f_α and f_{Fe} are derived by solving the set of equations:

$$\begin{aligned} Z_n &= X_{\alpha,n} + X_{Fe,n} + X_{0,n} = \\ &= f_\alpha \frac{Z_n}{Z_b} X_{\alpha,b} + f_{Fe} \frac{Z_n}{Z_b} X_{Fe,b} + \\ &\quad + \frac{Z_n}{Z_b} X_{0,b}, \\ [\alpha/Fe]_n - [\alpha/Fe]_b &= \log \left(\frac{X_{\alpha,n}}{X_{Fe,n}} \right) - \log \left(\frac{X_{\alpha,\odot}}{X_{Fe,\odot}} \right) \\ &\quad - \log \left(\frac{X_{\alpha,b}}{X_{Fe,b}} \right) + \log \left(\frac{X_{\alpha,\odot}}{X_{Fe,\odot}} \right) \\ &= \log \left(\frac{X_{\alpha,n}}{X_{Fe,n}} \right) - \log \left(\frac{X_{\alpha,b}}{X_{Fe,b}} \right) \\ &= \log \frac{f_\alpha}{f_{Fe}} \end{aligned} \quad (7)$$

The solutions f_α and f_{Fe} to (6) are:

$$\begin{aligned} f_{Fe} &= \frac{X_{\alpha,b} + X_{Fe,b}}{X_{\alpha,b} 10^{([\alpha/Fe]_n - [\alpha/Fe]_b)} + X_{Fe,b}}, \\ f_\alpha &= f_{Fe} 10^{([\alpha/Fe]_n - [\alpha/Fe]_b)} \end{aligned} \quad (8)$$

In the case in which the base model corresponds to the solar mixture (i.e., $X_{\alpha,b} = X_{\alpha,\odot}$ and $X_{Fe,b} = X_{Fe,\odot}$), the quantities f_α and f_{Fe} are given by:

$$\begin{aligned} f_{Fe} &= \frac{X_{\alpha,\odot} + X_{Fe,\odot}}{10^{[\alpha/Fe]_n} X_{\alpha,\odot} + X_{Fe,\odot}}, \\ f_\alpha &= f_{Fe} 10^{[\alpha/Fe]_n} \end{aligned} \quad (9)$$

and the mass fractions in the new mixture are:

$$\begin{aligned} X_{\alpha,n} &= f_\alpha \frac{Z_n}{Z_\odot} X_{\alpha,\odot}, \\ X_{Fe,n} &= f_{Fe} \frac{Z_n}{Z_\odot} X_{Fe,\odot}, \\ X_{0,n} &= \frac{Z_n}{Z_\odot} X_{0,\odot} \end{aligned} \quad (10)$$

Adopting the solar abundances of Grevesse & Sauval (1998), and assigning the elements N, O, Ne, Na, Mg, Si, S, Ca, and Ti to the *enhanced* group and Cr, Mn, Fe, Co, Ni, Cu, and Zn to the *depressed* group, we get $X_{\alpha,\odot} = 1.251 \times 10^{-2}$ and $X_{Fe,\odot} = 1.4 \times 10^{-3}$.

3.4. Specific response functions

Specific response functions allow to isolate the effect on line-strength indices due to variations of one element at once. The first to quantify this effect were TB95 who computed model atmospheres and synthetic stellar spectra along a 5-Gyr-old isochrone with solar metallicity. The model atmospheres were computed for three points along the isochrone representative of the evolutionary phases of dwarfs ($T_{eff} = 4575$ K, $\log g = 4.6$), turn-off (6200 K, 4.1), and giants (4255 K, 1.9). On each synthetic spectra, TB95 measured the absolute values I_0 for the original 21 Lick indices. Then they computed new model atmospheres, doubling the abundances of the dominant elements C, N, O, Mg, Fe, Ca, Na, Si, Cr, and Ti ($\Delta[X_i] = 0.3$) in turn, and derived the index changes ΔI . The index response for an increase of +0.3 dex of the i -th element abundance is defined as:

$$R_{0.3}(i) = \frac{1}{I_0} \frac{\partial I}{\partial [X_i]} 0.3 = \frac{\Delta I_{TB95}}{I_0}, \quad (11)$$

where I_0 and ΔI_{TB95} are, respectively, the index computed by TB95 for solar composition and the index change measured for a +0.3 dex abundance increase. Recently K05 have extended the work of TB95 to a wide range of

Table 2

Index	a	b	Index	a	b
CN1	1.536	0.0939	Fe5270	0.750	0.3796
CN2	1.373	0.0586	Fe5335	0.717	0.5359
Ca4227	0.491	0.6089	Fe5406	0.785	0.2249
G4300	0.880	0.9856	Fe5709	0.610	0.3613
Fe4383	0.757	0.9480	Fe5782	1.008	0.1879
Ca4455	1.564	0.5247	NaD	0.792	0.7805
Fe4531	0.600	0.9362	TiO1	—	—
C24668	1.080	4.1530	TiO2	2.722	0.0092
H β	0.936	-0.1275	H δ	0.663	-0.1094
Fe5015	0.783	1.4040	H γ	0.669	0.2911
Mg1	0.817	0.0040	H δ	0.461	0.8014
Mg2	0.822	0.0120	H γ	0.864	0.0899
Mgb	0.776	0.6049			

Notes: a and b are the coefficients of the linear transformation $EW_{\text{Lick}} = a \times EW_{\text{atmo}} + b$ adopted to transform the indices derived from the model atmospheres of Korn et al. (2005) into the Lick system.

metallicities and have included in their analysis the higher order Balmer lines (H γ and H δ) as well. We have adopted these new responses to compute our SSP models with α -enhanced composition.

As the index responses will be used in the following to correct solar-scaled SSP models based on FFs, we have first of all compared the solar-scaled indices computed by K05 for their model atmospheres with the FFs of Worthey et al. (1994). We have limited the comparison to metallicities $[Z/H] \geq 0$, as at lower metallicities the FFs, calibrated on Milky Way stars, reflect super solar $[\alpha/\text{Fe}]$ ratios. We observe that while in some cases there is a good match between FFs and model atmospheres, in other cases large deviations are present (see Fig. 1).

Mismatches between theoretical models and observations may be due both to uncertainties in the input physics of the model and to residual effects in the calibration of the model into the observed system (Chavez, Malagnini & Morossi 1996). We then wonder whether model indices should be transformed into the Lick system, in analogy with the transformation usually performed in the literature on measured indices through observation of standard stars in common with the Lick library (Worthey & Ottaviani 1997). We derive the linear transformation ($I_{\text{FF}} = a \times I_{\text{atmo}} + b$), which is needed to match the atmospheric indices with the FFs. The coefficients a and b of the transformation are given in Table 2. In Sect. 3.5 the index correction will be computed adopting the K05 responses revised in the following way:

$$\begin{aligned} \frac{\Delta I_{(\alpha, \text{Lick})}}{I_{(\alpha=0, \text{Lick})}} &= \frac{(a \times I_{\alpha} + b) - (a \times I_0 + b)}{a \times I_0 + b} = \\ &= \frac{a \times (I_{\alpha} - I_0)}{a \times I_0 + b}, \end{aligned} \quad (12)$$

where I_0 is the index from the solar scaled atmospheres, I_{α} is the index from the α -enhanced atmospheres, and $I_{(\alpha=0, \text{Lick})}$ and $\Delta I_{(\alpha, \text{Lick})}$ are the solar-scaled index and the index change transformed into the Lick system, respectively.

An important point to be assessed concerns the metallicity dependence of the indices, and more specifically the dependence of the fractional response $\Delta I/I$. We recall here that the behavior of the equivalent width of a line with respect to the abundance of an element is described by the curve of growth, and characterized by three different regimes: a linear part, where $EW \propto N$, for a small number of absorbers N (proportional to the metallicity Z); a saturated part, where $EW \propto \sqrt{\ln N}$, in the Doppler regime of saturated lines; and a collisionally broadened regime, described by $EW \propto \sqrt{N}$, for large N .

To assess in which regime the Lick indices are, in a first attempt we have analyzed the behavior of the K05 indices with global metallicity. In principle, such analysis would require keeping the temperature and the gravity fixed and only let the metallicity varying, while the K05 indices were computed for different $(T_{\text{eff}}, \log g)$ pairs at different metallicities. Nevertheless, T_{eff} and $\log g$ variations are small within each phase (see Table 2 in K05). By analyzing the index behavior, we observe that the Lick indices are not linearly related to Z . A viable explanation is that, at the Lick-IDS system resolution, the contribution to the index absorption strength from weak lines is negligible, as weak lines are likely to be flattened to the continuum or blended with stronger lines. In reverse, the major contribution to the index equivalent width derives from strong saturated absorption lines, for which it would be more appropriate to consider the flat part or the square root part of the curve of growth.

This evidence is strongly supported by preliminary results that we have obtained with the last version of the ATLAS code (ATLAS12, Kurucz 1993b), which is based on the opacity-sampling (OS) method. Following TB95 and K05, we have computed model atmospheres and synthetic spectra for a model with solar abundance ratios and for models in which the abundances of the elements C, N, O, Mg, and Fe have been changed by different amounts ($[X/H] = -0.2, +0.2, +0.3, +0.5$). In Figure 2 we plot the index as a function of the logarithmic (left panels) and linear (right panels) abundance of the index-dominating element for the indices (Mg₂, Mgb, Fe5335, Fe5270). For more details we refer to Annibali (2005). We observe that the behavior of the indices as a function of the element abundances is very well described by a functional form that is linear in $[X/H]$ ($I = a \times [X/H] + b$) or, equivalently, logarithmic in X ($I = a \times \log X/X_{\odot} + b$).

3.5. The ΔI correction

As explained in the previous section, specific response functions quantify the index change due to the deviation of one element from the solar composition. The total index

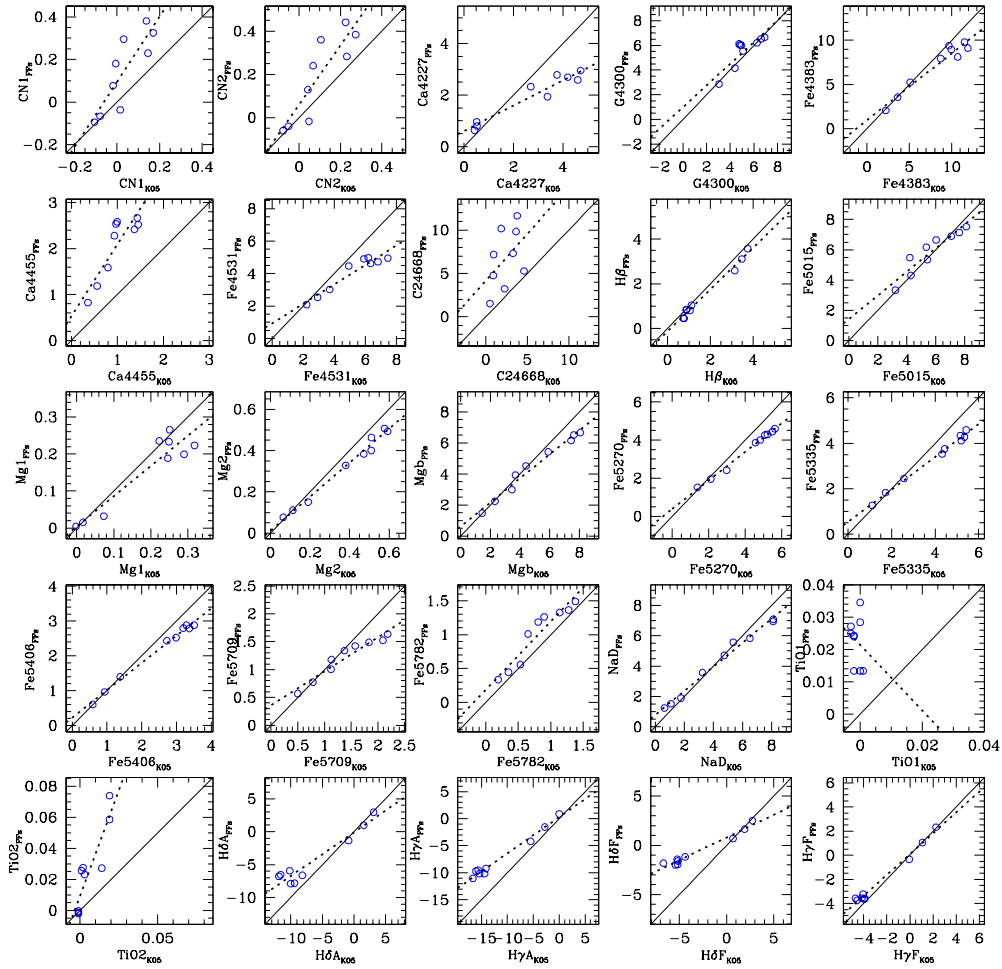


Fig. 1. Comparison between solar-scaled indices obtained by Korn et al. (2005) for their model atmosphere with fitting functions. The comparison is limited to metallicities $[Z/H] \geq 0$. The solid line is the one-to-one relation, while the dashed line is the performed fit to the data.

correction for a mixture in which several elements depart from the solar abundance path is derived through a linear combination of the specific responses, i.e., assuming that the total effect on the index can be expressed as the sum of the single effects due to the variation of one element at once. In the literature, different expressions to derive the index change on the basis of the same specific response functions have been proposed.

Using the TB95 responses, Trager et al. (2000a) propose the formula

$$\frac{\Delta I}{I_0} = \left\{ \prod_i [1 + R_{0.3}(X_i)]^{[X_i/H]/0.3} \right\} - 1 \quad (13)$$

for the fractional index variation, where $R_{0.3}(X_i) = \frac{1}{I_0} \frac{\partial I}{\partial [X_i]} 0.3$ is the fractional index change computed by TB95 for an increase of the i -th element abundance of 0.3 dex. The computations of TB95 are limited to the solar metallicity. Trager et al. (2000a) propose to extend the index correction to non-solar cases

with the reasonable assumption that the fractional index change is independent of metallicity.

Tantalo & Chiosi (2004a) adopt the same functional form to compute the index variations. TMB03 propose a different approach starting from the assumption that the line strength index is a linear function of the element abundance. TMB03 assume that Lick spectral features are in the linear regime of the curve of growth. They thus assume that $I \propto X_i$ and consequently $\ln I \propto [X_i]$ (note, however, that the latter implies $I \propto X_i^\alpha$), and then express the index through the Taylor series

$$\ln I = \ln I_0 + \sum_{i=1}^n \frac{\partial \ln I}{\partial [X_i]} \Delta [X_i] \quad (14)$$

However, as discussed in Sect. 3.4, at the Lick resolution the major contribution to the index line-strengths arises from strong saturated absorption lines, and a logarithmic functional form for the index behavior with element abundance may be more appropriate than a linear one. Then we express the index I through the Taylor expansion:

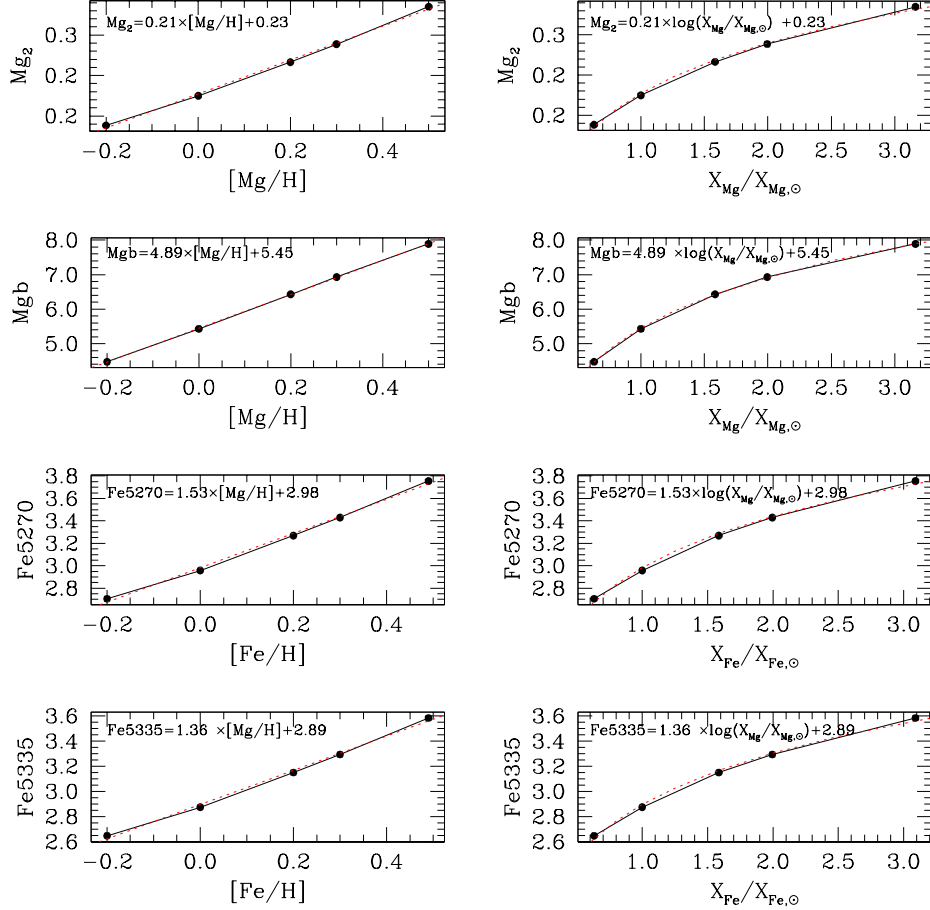


Fig. 2. Mg₂, Mgb, Fe5335, and Fe5270 indices as functions of the element abundance. In the left panels the index is plotted as a function of the logarithmic element abundance [X/H], while in the right panels as a function of the linear abundance X/X_⊕. Full circles are the model atmospheres computed with ATLAS12, and the solid line connects the models, while the dotted line is the performed fit, which is also given in the box.

$$I = I_0 + \sum_{i=1}^n \left[\frac{\partial I}{\partial [X_i]} \right]_0 \Delta[X_i]. \quad (15)$$

The fractional index change is

$$\frac{\Delta I}{I_0} = \sum_{i=1}^n \frac{1}{I_0} \left[\frac{\partial I}{\partial [X_i]} \right]_0 \Delta[X_i]. \quad (16)$$

The computations of K05 allow us to derive the fractional index change $\frac{\Delta I}{I_0}$ at different metallicities. We assume that we start from a mixture where the total metallicity Z and the element abundances are

$$X_{i,0} = f_b \frac{Z}{Z_{\odot}} X_{i,\odot}, \quad (17)$$

where f_b accounts for the [α/Fe] bias of the stellar libraries (see Sect. 3.7), and it is the enhancement/depression factor with respect to the solar-scaled abundance for that

metallicity Z. If now we perturb the abundance of the i-th element, the new mass fraction is given by

$$X_i = f_i X_{i,b} = f_i f_b \frac{Z}{Z_{\odot}} X_{i,\odot}, \quad (18)$$

and the logarithmic abundance change is

$$\Delta[X_i] = \log \frac{X_i}{X_{i,0}} = \log f_i. \quad (19)$$

For a given Z, the expression for the fractional index change becomes

$$\frac{\Delta I}{I_0}|_Z = \sum_{i=1}^n \frac{K_{0.3,Z}}{0.3} \log f_i, \quad (20)$$

where $K_{0.3,Z}$ are the new response functions $\Delta I/I_0$ computed by K05 for an increase of the element abundance of +0.3 dex.

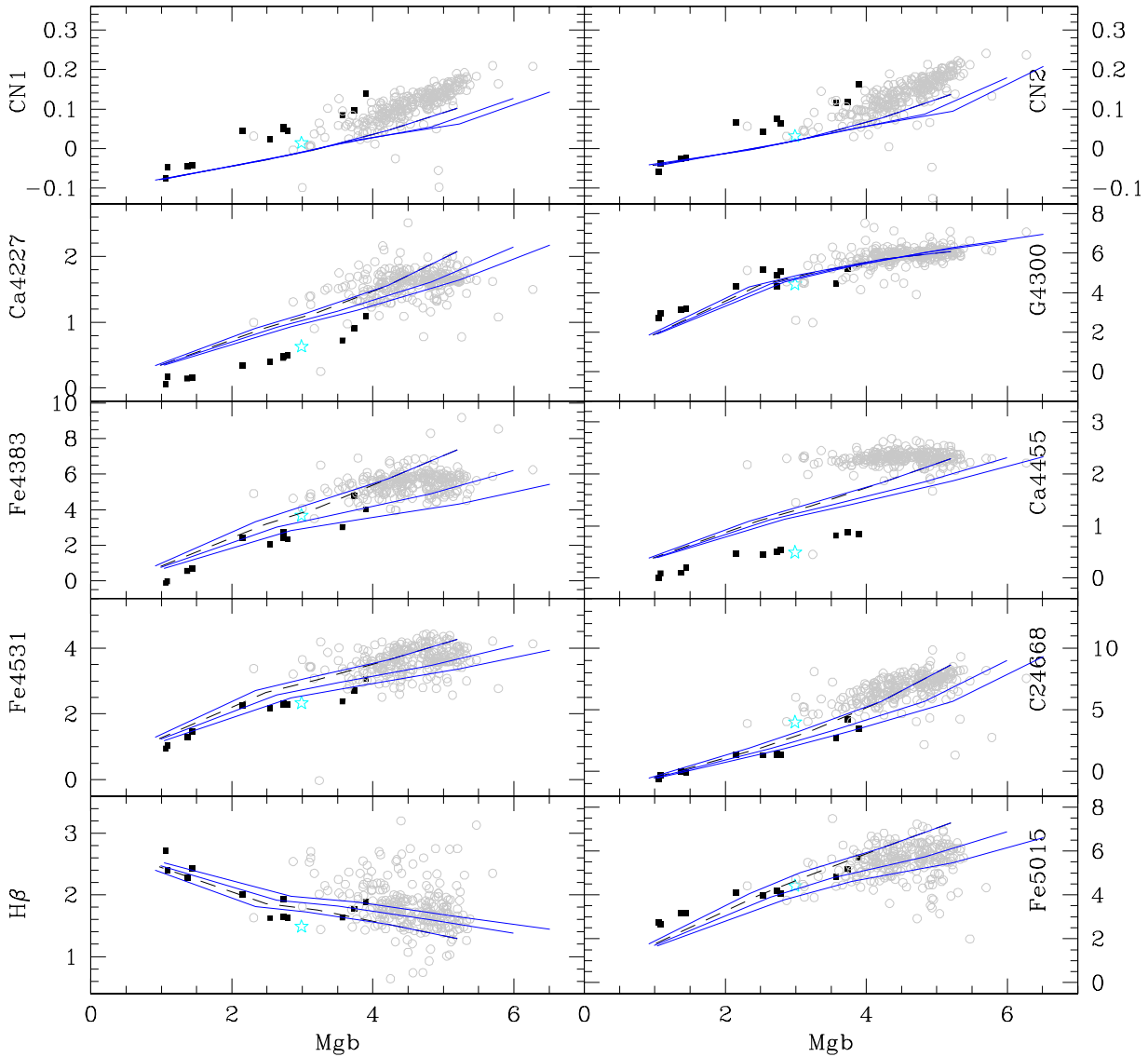


Fig. 3. Mgb index versus the other 24 Lick indices for a fixed age of 12 Gyr and metallicities in the range $0.0004 \leq Z \leq 0.05$. The metallicity increases for increasing Mgb values. The long dashed line is the base model. The solid line represents the α -enhanced models computed for different $[\alpha/\text{Fe}]$ ratios (0, 0.3, 0.5), assuming that the index behavior is logarithmic with element abundance. Models with the larger Mgb index correspond to larger $[\alpha/\text{Fe}]$ ratios. Full squares and open stars are the globular clusters data and the integrated bulge light, respectively, in Puzia et al. (2002). Open circles are our data sample (Papers I + II).

3.6. The final SSP model

With the functional dependence of $\Delta I/I$ on element abundance described by Eq. (20), the new SSP indices are computed following the same procedure adopted by TMB03.

We split the basic SSP model into three evolutionary phases, dwarfs (D), turnoff (TO), and giants (G). Gravity determines the separation between dwarfs ($\log g > 3.5$) and giants ($\log g < 3.5$). Following TMB03, we used the fixed temperature of 5000 K to separate the turn-off re-

gion from the cool dwarfs on the main sequence, independently of age and metallicity. TMB03 have also demonstrated that the impact of this choice on the final SSP model is small. The Lick indices of the base model are computed for each evolutionary phase separately; this is done by integrating the continua and line fluxes along each phase, and finally deriving the indices I_D , I_{TO} , and I_G from the continua $F_{C,D}$, $F_{C,\text{TO}}$, and $F_{C,G}$ and the line fluxes $F_{R,D}$, $F_{R,\text{TO}}$, and $F_{R,G}$ of the three phases. At this point the index is corrected for each phase, adopting the K05

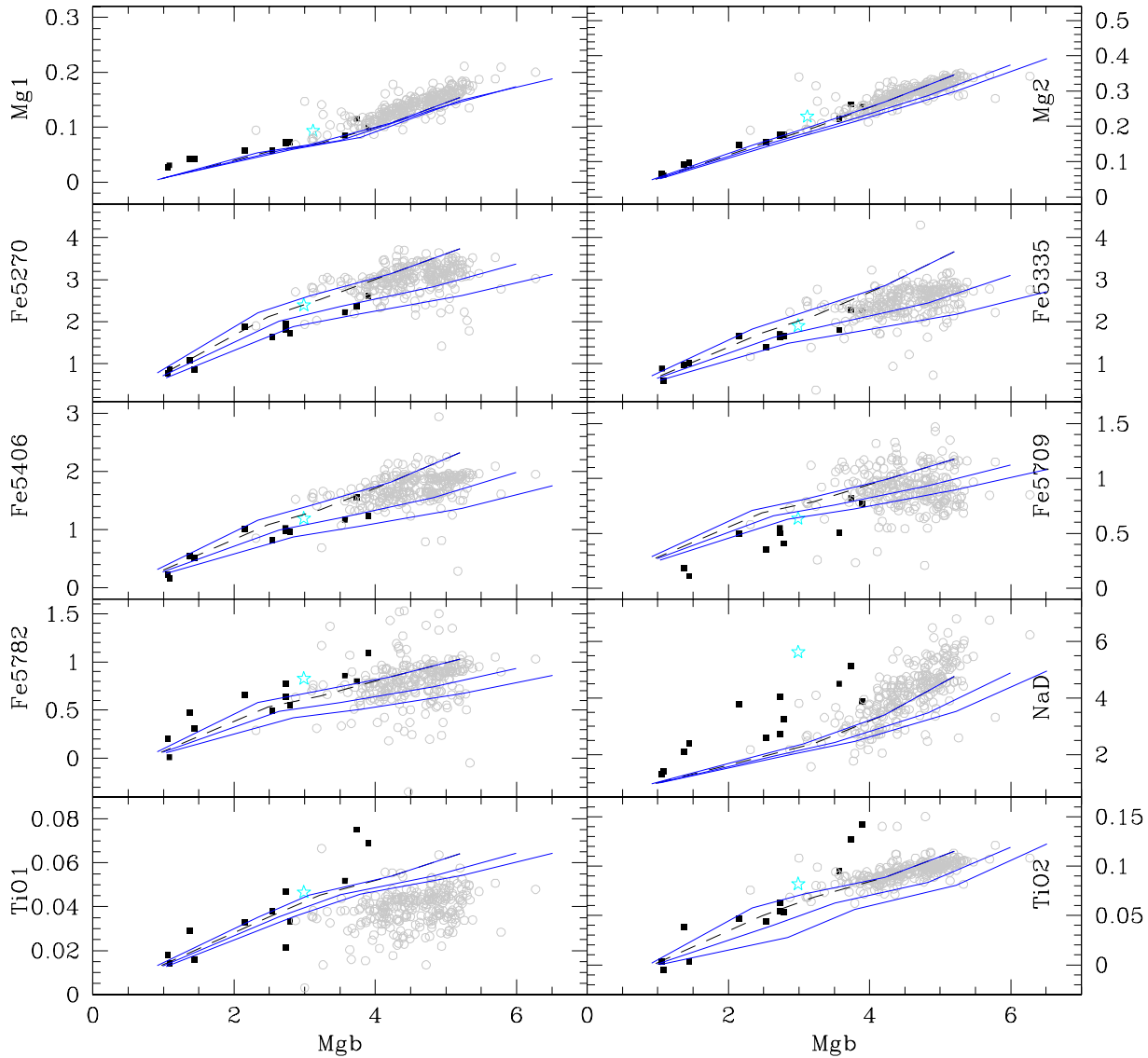


Fig. 4. Same as Fig. 3.

responses in the appropriate phase and computing the ΔI as described in Sect. 3.5. Once the new corrected indices I_D^* , I_{TO}^* , and I_G^* are computed, the final α -enhanced SSP index is obtained through two different expressions, depending on if the index is defined as EW or mag.

EW:

$$\begin{aligned}
 & - \left[\frac{\left(1 - \frac{I_G^*}{\Delta\lambda}\right) F_{C,G}}{F_{C,D} + F_{C,TO} + F_{C,G}} \right] \Delta\lambda = \\
 & = \frac{I_D^* \times F_{C,D} + I_{TO}^* \times F_{C,TO} + I_G^* \times F_{C,G}}{F_{C,D} + F_{C,TO} + F_{C,G}}, \quad (21)
 \end{aligned}$$

Magnitude:

$$\begin{aligned}
 I_{SSP} &= \left[1 - \frac{F_{R,D} + F_{R,TO} + F_{R,G}}{F_{C,D} + F_{C,TO} + F_{C,G}} \right] \Delta\lambda = \\
 &= \left[1 - \frac{\left(1 - \frac{I_D^*}{\Delta\lambda}\right) F_{C,D} + \left(1 - \frac{I_{TO}^*}{\Delta\lambda}\right) F_{C,TO}}{F_{C,D} + F_{C,TO} + F_{C,G}} \right] \Delta\lambda +
 \end{aligned}$$

$$\begin{aligned}
 I_{SSP} &= -2.5 \log \left(\frac{F_{R,D} + F_{R,TO} + F_{R,G}}{F_{C,D} + F_{C,TO} + F_{C,G}} \right) = \\
 &= 1 - 2.5 \log \frac{10^{I_D^*} F_{C,D} + 10^{I_{TO}^*} F_{C,TO} + 10^{I_G^*} F_{C,G}}{F_{C,D} + F_{C,TO} + F_{C,G}}, \quad (22)
 \end{aligned}$$

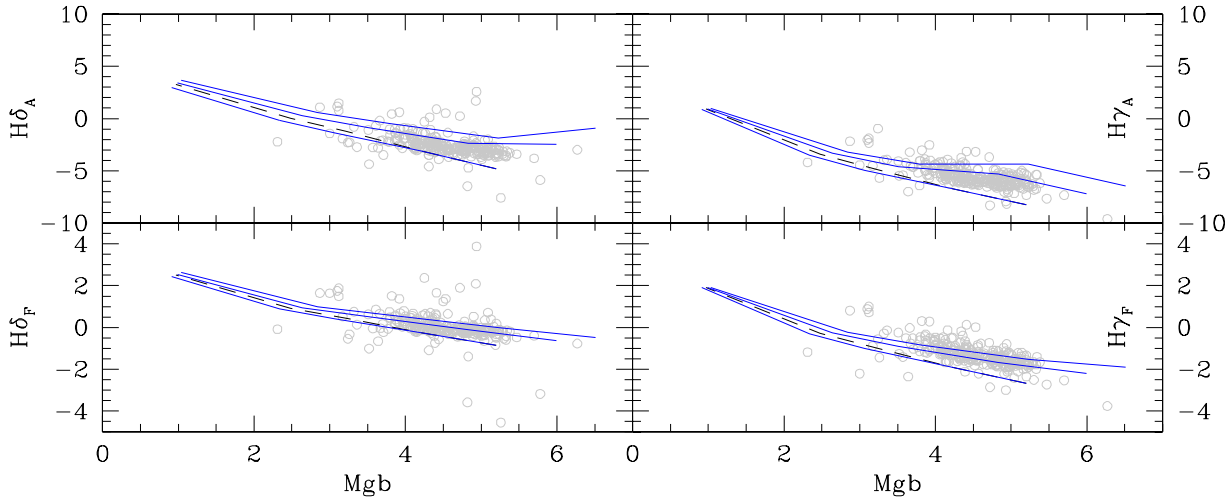


Fig. 5. Same as Fig. 3.

3.7. The α/Fe bias of stellar libraries

As discussed by TMB03, an additional complication in the construction of the α -enhanced SSP models is due to the fact that the fitting functions, on which the standard models are based, are constructed from empirical stellar libraries that reflect the chemical enrichment history of the Milky Way. More specifically, metal poor halo stars ($[\text{Fe}/\text{H}] < -1$), which formed at early epochs in a short timescale, are characterized by supersolar $[\alpha/\text{Fe}]$ ratios (~ 0.3). Metal rich disk stars, which formed on longer timescales and were enriched by Type Ia supernovae, instead exhibit an $[\alpha/\text{Fe}]$ trend that decreases from 0.3 to solar for increasing metallicity (Edvardsson et al. 1993; Fuhrmann 1998). The result is that the base models constructed on the FFs do not have solar abundance ratios at every metallicity, but reflect the α/Fe bias of the FFs at subsolar metallicity. In Table 3, we show the $[\alpha/\text{Fe}]$ values adopted for the bias, which are obtained by interpolating the values given in Table 3 of TMB03 to our metallicity grid. For a model of given metallicity and total $[\alpha/\text{Fe}]$, the $[\alpha/\text{Fe}]_b$ of the bias is the starting point for the computation of the f_i factors according to Eqs. 8 and 9. Summarizing, we have computed new α -enhanced SSP models adopting the K05 specific response functions. For comparison with TMB03, we present the results for models computed for a mixture in which the enhanced elements are N, O, Ne, Na, Mg, Si, S, Ca, and Ti, while the depressed ones are Cr, Mn, Fe, Co, Ni, Cu, and Zn.

We plot the Mg b index versus the other 24 Lick indices for a fixed age of 12 Gyr and total metallicities in the range $0.0004 \leq Z \leq 0.05$ in Figs. 3, 4, and 5. The metallicity increases for increasing Mg b values. The α -enhanced models represented are computed for different $[\alpha/\text{Fe}]$ ratios (0, 0.3, 0.5). Larger $[\alpha/\text{Fe}]$ ratios correspond to larger Mg b indices. In the same figure we have plotted the globular clusters data (Puzia et al. 2002), the integrated bulge

Table 3. The α/Fe bias in the Milky Way.

Z	0.0004	0.004	0.008	0.02	0.05
$[\alpha/\text{Fe}]$	0.22	0.14	0.1	0.	0.

light (Puzia et al. 2002), and the 65 elliptical galaxies of the sample of Papers I + II. The plot is analogous to that presented in Fig. 2 of TMB03 and Fig. 3 of K05.

3.8. Calibration of an enhancement-independent index

We have checked if the $[\text{MgFe}]$ index, proposed by G93 and revised by TMB03, is still a tracer of total metallicity independently of the α -enhancement. G93 defines the index

$$[\text{MgFe}] = \sqrt{\text{Mgb} < \text{Fe} >} \quad (23)$$

with

$$< \text{Fe} > = \frac{1}{2}(\text{Fe}5270 + \text{Fe}5335), \quad (24)$$

while TMB03 propose the new index $[\text{MgFe}]'$, whose definition is still given by Eq. (23), although the $< \text{Fe} >$ index is replaced by

$$< \text{Fe} > = (0.72 \cdot \text{Fe}5270 + 0.28 \cdot \text{Fe}5335). \quad (25)$$

In Fig. 6 we plot the indices Mg b, $< \text{Fe} >$, $[\text{MgFe}]$, and $[\text{MgFe}]'$ as a function of $[\alpha/\text{Fe}]$ for our new SSP models.

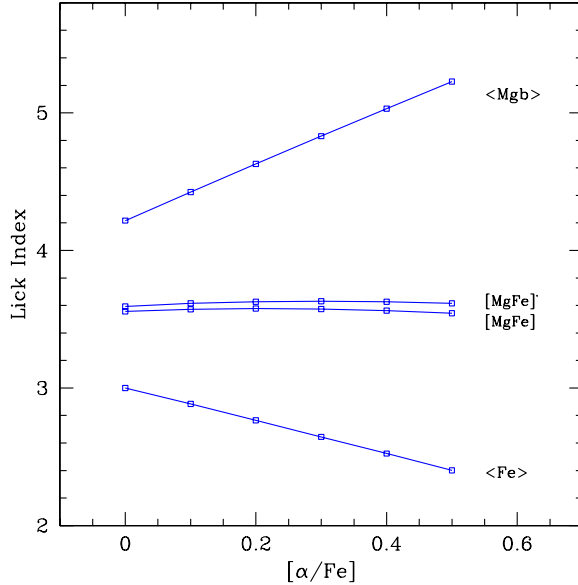


Fig. 6. Lick indices as a function of $[\alpha/\text{Fe}]$ ratio at fixed solar metallicity. We plot the indices Mgb , $\langle \text{Fe} \rangle = \frac{1}{2}(\text{Fe5270} + \text{Fe5335})$, $[\text{MgFe}]$, and $[\text{MgFe}]'$ (see text for details) for a 12-Gyr-old SSP of our new α -enhanced models.

In all the models, the Mgb index increases with the α -enhancement, while $\langle \text{Fe} \rangle$ decreases. On the other hand, the $[\text{MgFe}]$ and $[\text{MgFe}]'$ indices remain essentially constant. More specifically, the fractional variations of $[\text{MgFe}]$ and $[\text{MgFe}]'$ amount to ~ -0.004 and ~ 0.006 , respectively, passing from $[\alpha/\text{Fe}] = 0$ to $[\alpha/\text{Fe}] = 0.5$.

3.9. Comparison with TMB03 SSPs

We have compared our new SSP models with those of TMB03. Since both models are based on the fitting functions of Worthey et al. (1994) and Worthey & Ottaviani (1997), the possible differences between the models for solar-scaled compositions must be due to the different evolutionary tracks adopted. For α -enhanced compositions, an additional difference is the new index dependence on element abundance introduced in our models (see Sect. 3.5).

In Fig. 7 we plot the $\text{H}\beta$ and $[\text{MgFe}]'$ indices predicted by our models and those of TMB03 for solar total metallicity, ages in the range 1–15 Gyr, and $[\alpha/\text{Fe}] = 0, 0.5$, plus the TMB03 models for $[\text{Z}/\text{H}] = 0.35$ and $[\alpha/\text{Fe}] = 0$. In particular, we observe that our solar metallicity models are between the $[\text{Z}/\text{H}] = 0$ and $[\text{Z}/\text{H}] = 0.35$ TMB03 models. Thus we expect our models to yield lower metallicities for the same line-strength index data. The comparison is also showed in Table 4. We compare our models with those of TMB03 and Tantalo & Chiosi (2004a, (TC04) for solar metallicity, $[\alpha/\text{Fe}] = 0$, and ages = 5, 10 Gyr, for some commonly used indices. We observe that there is a significant difference in the metallic indices, in particular the

Table 4. Comparison with SSPs in the literature

	$\text{H}\beta$	Mg_2	Mgb	Fe5270	Fe5335	$[\text{MgFe}]'$
<hr/>						
5 Gyr						
US	1.95	0.23	3.60	2.86	2.59	3.17
TMB03	1.99	0.21	3.18	2.83	2.52	2.95
TC04	1.90	0.23	3.30	2.90	2.63	3.06
<hr/>						
10 Gyr						
US	1.62	0.26	4.08	3.06	2.79	3.49
TMB03	1.70	0.23	3.58	2.98	2.66	3.22
TC04	1.50	0.27	3.76	3.12	2.85	3.38

Mgb . Our models predict Mgb indices that are quite larger than TMB03, and this results in higher $[\text{MgFe}]'$. The TC04 models are instead between our models and the TMB03 ones. Bluer metallic indices are probably the results of hotter stellar tracks. In particular it is well known that the Girardi et al. (2000) tracks used in the TC04 models predict warmer red giant branches (see, e.g., Bruzual & Charlot 2003).

To perform a more direct and quantitative comparison, we have considered the ($\text{H}\beta$, Mgb , and $\langle \text{Fe} \rangle$) indices for some selected TMB03 models of a given age, $[\text{Z}/\text{H}]$, and $[\alpha/\text{Fe}]$, and have fitted those indices with our models. This allows us to directly compare the (age, $[\text{Z}/\text{H}]$, and $[\alpha/\text{Fe}]$) solutions provided by our models and those of TMB03 for the same index triplet. Our test shows that there are significant differences in the derived stellar population parameters. The major discrepancy concerns metallicity: our models provide metallicities that are systematically lower (up to 0.2 dex) than those predicted by the TMB03 models. On the other hand, our derived ages tend to be older (10% higher at 10 Gyr). The $[\alpha/\text{Fe}]$ ratios are instead in good agreement. We only observe that for high $[\alpha/\text{Fe}]$ ratios (~ 0.5), we tend to predict values that are larger by $\sim 20\%$. The same metallicity-age discrepancy has also been discussed by Denicolo' et al. (2005b) when comparing the TMB03 models with those of Worthey (1994): fitting the line strength index data of the galaxy NGC 3379 with both the set of models, they derived a higher metallicity ($\Delta[\text{Fe}/\text{H}] = 0.08$) and a younger age ($\Delta \text{age} = -0.5$ Gyr) with the TMB03 SSPs than with the Worthey (1994) ones.

4. Derivation of stellar population parameters

4.1. The line-strength index diagnostic

The use of absorption-line indices has proven to be a powerful tool in the derivation of ages and metallicities of unresolved stellar populations (e.g., Worthey 1994). To this purpose it is important to identify those absorption features, among the Lick indices, that possess a marked sen-

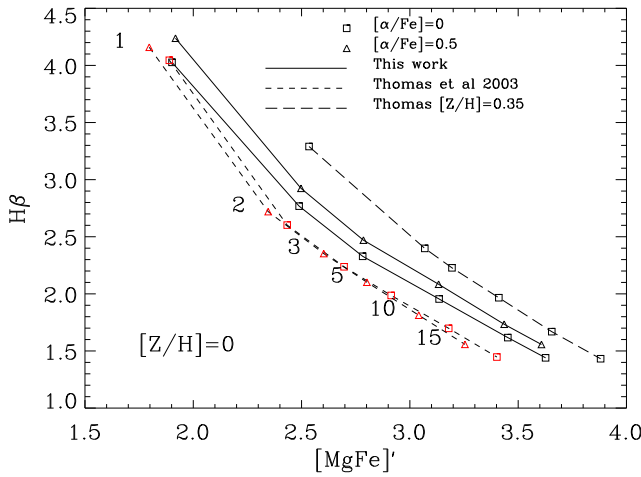


Fig. 7. Comparison of our SSP models with the models of TMB03 for solar total metallicity, ages in the range 1–15 Gyr, and $[\alpha/\text{Fe}]=0, 0.5$. In the $\text{H}\beta$ vs. $[\text{MgFe}]'$ plane, our models are denoted with the solid line, the TMB03 models with the short-dash line. The long-dash line is for the TMB03 models at $[\text{Z}/\text{H}]=0.35$. We observe that our solar metallicity models are between the $[\text{Z}/\text{H}]=0$ and $[\text{Z}/\text{H}]=0.35$ TMB03 models.

sensitivity either to abundance or age, that are not strongly affected by uncertainties in the measurement process, and, finally, that can be described by fairly robust models. Among the Balmer lines, which, measuring the presence of warm A-type stars, can be used as age indicators, the $\text{H}\beta$ index turns out relatively insensitive to abundance ratio variations, but it may be contaminated by nebular emission. In reverse, higher order Balmer lines, less affected than $\text{H}\beta$ by emission infilling (in particular the $\text{H}\delta$ less than the $\text{H}\gamma$), are not independent from abundance ratio variations, as shown in Sect. 3.

Line-strength indices, like the Mg and Fe indices, derived from metallic lines are mainly sensitive to element abundances, but they also depend on age. In particular, we have shown in Sect. 3.8 that the $[\text{MgFe}]$ and $[\text{MgFe}]'$ indices are good tracers of total metallicity and are almost completely independent of α/Fe ratio variations. Thus, a three-dimensional space defined by a Balmer absorption line, the $[\text{MgFe}]$ (or $[\text{MgFe}]'$), and a metallic index sensitive to α -enhancement (like Mgb) demonstrates itself to be a suitable diagnostic tool for the derivation of ages, metallicities, and $[\alpha/\text{Fe}]$ ratios.

In Fig. 8, we plotted four projections of the spaces defined by $(\text{H}\beta, [\text{MgFe}]', \text{Mgb})$, $(\text{H}\gamma_F, [\text{MgFe}]', \text{Mgb})$, and $(\text{H}\delta_F, [\text{MgFe}]', \text{Mgb})$. In the planes $\text{Mgb} - [\text{MgFe}]'$, $\text{H}\beta - [\text{MgFe}]'$, $\text{H}\gamma_F - [\text{MgFe}]'$, and $\text{H}\delta_F - [\text{MgFe}]'$, we superposed the SSP models on the line-strength indices derived for our sample within $r_e/8$. Galaxies with different detection levels of the $[\text{OIII}]\lambda 5007$ emission line are plotted using different symbols. In this plot we show only 62 out of the initial sample of 65 galaxies. We have excluded: the

Seyfert galaxy IC 5063 because of the presence of very strong emission lines, which prevented us from deriving reliable absorption line indices; NGC 6875, which lacks a measure of velocity dispersion (consequently the indices have not been corrected for this effect), and NGC 2962, which clearly shows calibration problems in the higher order Balmer indices and presents significant emission that can affect the $\text{H}\beta$. These three galaxies will not be included in our results. In the Balmer indices vs. $[\text{MgFe}]'$ planes, models of constant age (almost horizontal lines) and of constant metallicity (almost vertical lines) are fairly well separated as a result of the markedly different sensitivity of the Balmer index to age and of the $[\text{MgFe}]'$ index to metallicity (see Worthey 1994). The effect of α -enhancement is that of slightly strengthening the $\text{H}\beta$ feature. Though small, the variation at old ages corresponds to a few Giga years. On the contrary, $[\text{MgFe}]'$ is almost unaffected, due to the opposite response of Mg and Fe indices to α -enhancement. The $\text{H}\beta$ vs. $[\text{MgFe}]'$ plane, where the enhanced SSPs are almost superposed on the standard ones, is in principle well suited to directly reading off ages and total metallicities almost independently of abundance ratio effects. In the $\text{H}\beta$ vs. $[\text{MgFe}]'$ plane, but also in the other planes defined by high order Balmer lines, the data cluster in the lower right region of the diagram, between solar and twice solar metallicity models, and at old ages. A tail of objects extends at higher $\text{H}\beta$ values and, as already noticed by Longhetti et al. (2000), does not follow a line of constant metallicity. A large scatter in age is observed, and galaxies with equivalent-SSP ages of few Gyrs are present.

There are, in particular, few galaxies that fall outside the models at very high $\text{H}\beta$ values, even extrapolating the models at metallicities higher than $Z=0.05$: NGC 1052, NGC 3136, NGC 5266, and NGC 2911. We have labeled these objects in all the four panels to better understand the origin of the discrepancy. In particular we want to know if the high $\text{H}\beta$ values are caused by an overestimation of the emission correction or are rather due to intrinsic properties. We observe that NGC 3136 has high values for all the three Balmer indices. We note in particular that while the $\text{H}\beta$ has been corrected for emission, $\text{H}\gamma_F$ and $\text{H}\delta_F$ have not been. Thus the plotted $\text{H}\gamma_F$ and $\text{H}\delta_F$ are lower limits, and by applying the (small) emission correction to them, we would get even higher values. Given the high quality and the high S/N of the spectrum also, we conclude that the observed strong Balmer lines for NGC 3136 are a real effect. As noted by Bressan et al. (1996) and Longhetti et al. (2000), a galaxy in which a recent burst of star formation is superimposed on an old stellar population can fall above the $\text{H}\beta - [\text{MgFe}]$ region occupied by the SSPs. The reason is that if in the secondary burst the gas metallicity was higher than the metallicity of the old population, the galaxy moves vertically toward the top of the $\text{H}\beta - [\text{MgFe}]$ plane. Thus, it is likely that the position of NGC 3136 in the $\text{H}\beta - [\text{MgFe}]'$ plane is due to the occurrence of secondary bursts of star formation.

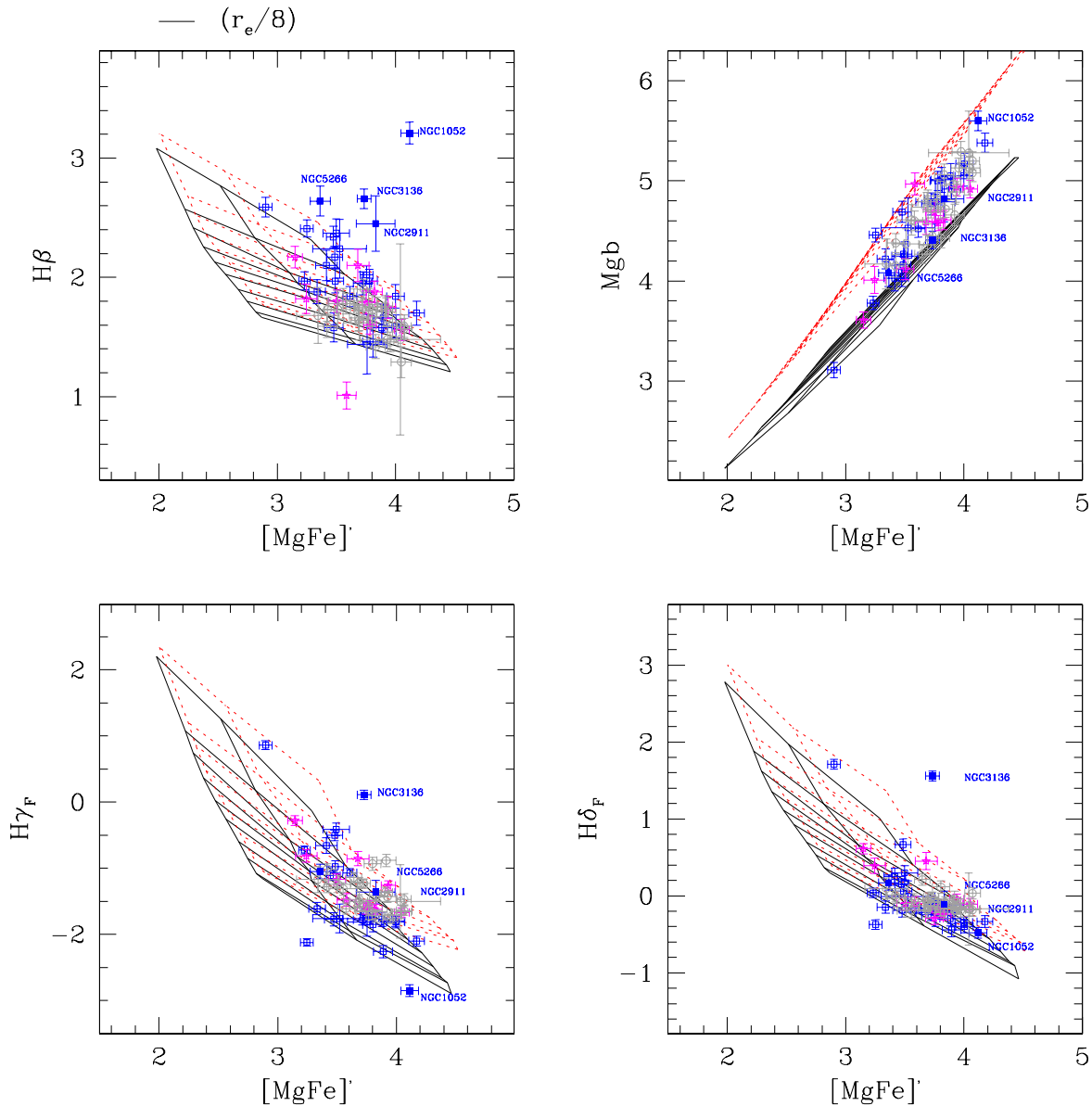


Fig. 8. Lick line-strength indices ($r_e/8$ aperture) of our sample compared with SSP models with metallicities $Z=0.008, 0.02$, and 0.05 , ages in the range $(2-15)$ Gyr, and $[\alpha/\text{Fe}]=0$ (solid line) and 0.4 (dotted line). We have plotted $H\beta - [\text{MgFe}]'$ (top left panel), $Mgb - [\text{MgFe}]'$ (top right), $H\gamma_F - [\text{MgFe}]'$ (bottom left), and $H\delta_F - [\text{MgFe}]'$ (bottom right) planes. The metallicity increases for increasing $[\text{MgFe}]'$ values, while the age increases for decreasing Balmer index. Vertical lines in the Balmer index vs. $[\text{MgFe}]'$ plane are models of constant metallicity, while horizontal lines are models of constant age. The data have been plotted with different symbols according to their emission properties: open circles for $[\text{OIII}\lambda 5007]$ emission detected under 1σ , triangles for emission between 1 and 2σ , and squares for $> 2\sigma$. The galaxies IC 5063, NGC 6875, and NGC 2962 have been excluded from the original sample of 65 galaxies.

The situation seems to be different for NGC 1052, NGC 5266, and NGC 2911. They all show high $H\beta$ values, but $H\gamma_F$ and $H\delta_F$ fall within the models (NGC 5266 and NGC 2911) or are too low ($H\gamma_F$ for NGC 1052). The observed inconsistency among the Balmer lines seems to be due to an overestimation of the $H\beta$ emission, with consequent overcorrection of the index. Given the accurate subtraction of the continuum around $H\alpha$ performed to de-

termine the emission (see Papers I and II), the only viable explanation for the high $H\beta$ emission is the presence of significant dust extinction: in this case the $FH\alpha/FH\beta$ ratio is higher than 2.86 , which is the value adopted throughout our analysis. Indeed HST observations have revealed dust absorption features in the center of NGC 1052 (van Dokkum & Franx 1995; Gabel et al. 2000); NGC 2911 is a disk dominated S0 with an important dust component

(Michard & Marchal 1994), and NGC 5266 is an HI-rich elliptical galaxy with a dust ring along the minor axis (Varnas et al. 1987; Morganti et al. 1997).

The index errors displayed in Fig. 8 have been obtained adding a Poissonian fluctuation to each spectrum and generating a set of 1000 Monte Carlo modifications (see Papers I and II). The error in the $H\beta$ index does not include the systematic uncertainties in the emission correction due to the choice of a particular template for the continuum subtraction and of a $FH\alpha/FH\beta$ ratio. Thus, we warn the reader that the $H\beta$ error bars plotted in Fig. 8 may be underestimated.

In the $Mgb - [\text{MgFe}]'$ plane, models of constant age and metallicity are almost degenerate, while the effect of the enhancement is well separated. We observe in particular that the bulk of data is confined between $[\alpha/\text{Fe}] = 0$ and $[\alpha/\text{Fe}] = 0.4$. Furthermore, there is a trend for galaxies with larger $[\text{MgFe}]'$ values to lie closer to the enhanced models than to the standard ones, suggesting a correlation between metallicity and α/Fe enhancement. The three-dimensional spaces described in this section will be used in our following analysis to derive ages, metallicities, and $[\alpha/\text{Fe}]$ ratios for our sample of galaxies. For this purpose we have devised a simple but robust algorithm, which we describe in the next section.

4.2. The probability distribution of the physical parameters

A SSP model of given age, metallicity, and α/Fe ratio corresponds to a point in a multi-dimensional space defined by the line-strength indices. If we exclude ages older than ~ 17 Gyr, where a blueing of the indices may be introduced by the presence of Horizontal Branch (HB) stars even at high metallicity, there is a unique correspondence between the index multiplet and a point in the age, metallicity, and $[\alpha/\text{Fe}]$ parameter space. In principle, one could chose three arbitrary indices and, by comparison with SSP models, derive the (age, Z , $[\alpha/\text{Fe}]$) solution. Nevertheless, as discussed in the previous section, some combinations of indices among the Lick set are more useful than others to disentangle the age-metallicity degeneracy, and thus turn out to be particularly suitable for deriving the stellar population parameters. More specifically, for our analysis we select the three dimensional spaces defined by $(H\beta, \langle \text{Fe} \rangle, Mgb)$, $(H\gamma_F, \langle \text{Fe} \rangle, Mgb)$, and $(H\delta_F, \langle \text{Fe} \rangle, Mgb)$. Once the index 3D space has been defined, the stellar population parameters are derived according to the following procedure.

Let us call (x_0, y_0, z_0) the observed point in the index space and $(\sigma_{x_0}, \sigma_{y_0}, \sigma_{z_0})$ the associated error. For each point (t, Z, α) in the (age, metallicity, α/Fe enhancement) space (G space), we can define the probability density that the generic SSP model $(x_{(t,Z,\alpha)}, y_{(t,Z,\alpha)}, z_{(t,Z,\alpha)})$ is the solution to the observed line-strength indices. In particular, if the errors are Gaussian, the probability density assumes the expression:

$$P_{t,Z,\alpha} = \frac{1}{\sqrt{(2\pi)^3 \sigma_{x_0} \sigma_{y_0} \sigma_{z_0}}} \exp \left[-\frac{1}{2} \left(\frac{x - x_0}{\sigma_x} \right)^2 - \frac{1}{2} \left(\frac{y - y_0}{\sigma_y} \right)^2 - \frac{1}{2} \left(\frac{z - z_0}{\sigma_z} \right)^2 \right]. \quad (26)$$

Equation (26) allows us to construct a probability density map $P_{t,Z,\alpha}$ defined on the three dimensional grid (t, Z, α) .

In Fig. 9, we show the contour levels in the (t, Z) plane, enclosing the solutions that are within one σ (in the three indices) from the observed values for some galaxies of our sample, as an example. Each panel refers to a different galaxy, and the three curves refer to the solutions obtained with the different triplets adopted, i.e., $H\beta, \langle \text{Fe} \rangle, Mgb$; $H\gamma_F, \langle \text{Fe} \rangle, Mgb$; and $H\delta_F, \langle \text{Fe} \rangle, Mgb$. The most probable solution in each index triplet is obtained by finding the maximum of the $P_{t,Z,\alpha}$ function.

Figure 9 shows that measurement errors combine with the relative index sensitivity to age and metallicity variations (the age metallicity-degeneracy). Levels of constant probability define a narrow elongated region of anti-correlation between age and metallicity solutions. Some authors have shown this effect by using Montecarlo simulations to generate a mock catalog of synthetic galaxies (e.g., Thomas et al. 2005). Notice that the age-metallicity degeneracy introduces an asymmetry in the errors of the solution, as a Gaussian error in the measured indices translates into a non-Gaussian error in the solution. We have used the three triplets to minimize spurious observational effects in the age indicator $H\beta$, which may be affected by emission filling. For each galaxy we combined only those index triplets that provide more reliable results, depending on the strength of the present emission (see below).

For most of the sources, the contour levels of the three index spaces possess a clear region of intersection. This indicates that models predict consistent results. However, there are galaxies for which the three G spaces do not have common solutions (within one- σ , if we consider two- σ , then there are always common solutions, but the uncertainty is large). In particular, for some galaxies, $H\beta$ provides solutions that are really detached from those provided by the other two age indicators. As discussed in Sect. 4.1, discrepancies between the $H\beta$ and the higher order Balmer lines could be due to problems in the derivation of the emission correction.

For each 3D index space, the solution is computed adopting a subspace (G^*) defined by $P_{t,Z,\alpha} > f \times P_{max}$, and performing an average on the (G^*) values weighted for the probability density:

$$t_\mu = \frac{\iiint_{G^*} t P(t, Z, \alpha) dt dZ d\alpha}{\iiint_{G^*} P(t, Z, \alpha) dt dZ d\alpha} \quad (27)$$

$$Z_\mu = \frac{\iiint_{G^*} Z P(t, Z, \alpha) dt dZ d\alpha}{\iiint_{G^*} P(t, Z, \alpha) dt dZ d\alpha}$$

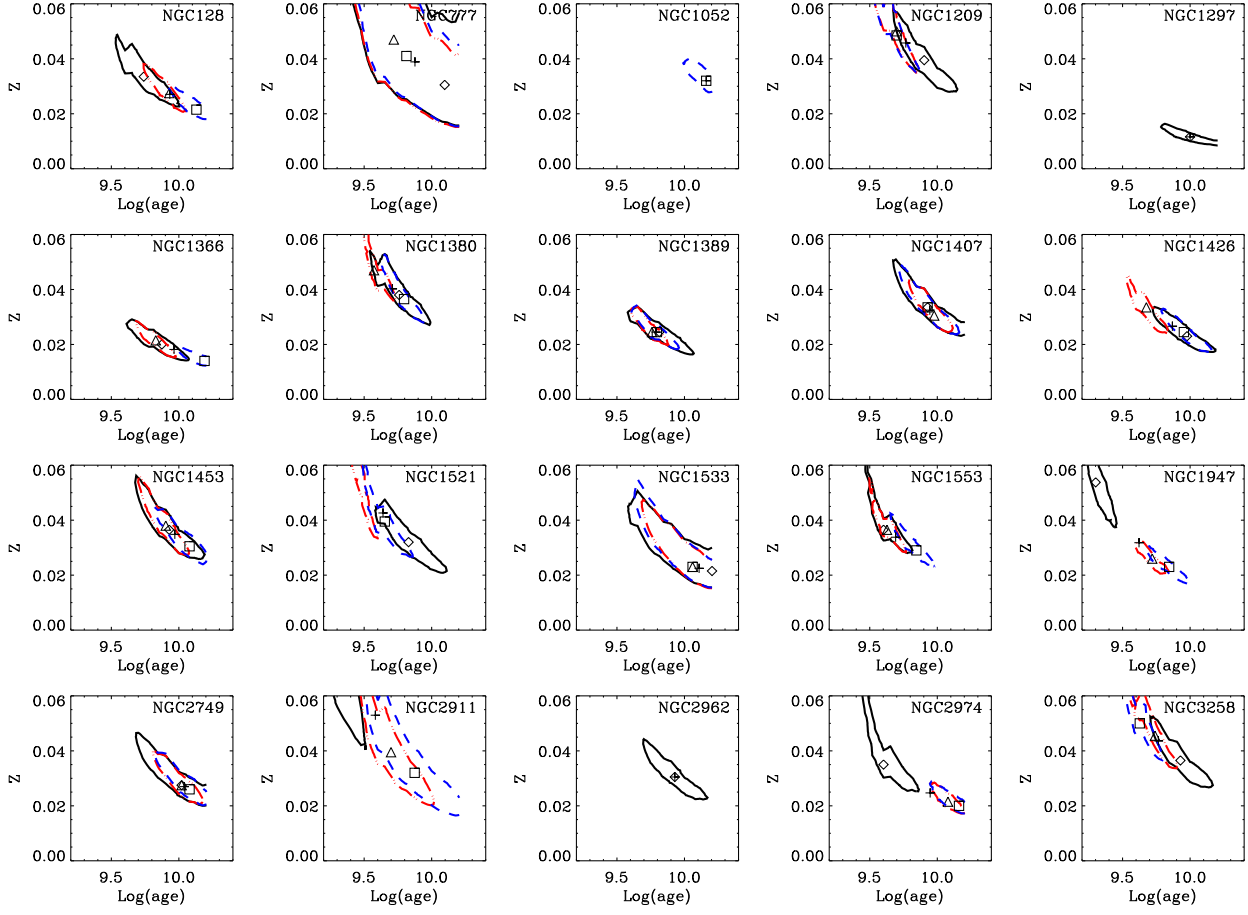


Fig. 9. Example of contour levels enclosing solutions that are within one σ from the observed value. Black solid lines are for $(H\beta, \langle Fe \rangle, Mgb)$ triplets, red dotted lines for the $(H\gamma_F, \langle Fe \rangle, Mgb)$ triplets, and blue dashed lines for the $(H\delta_F, \langle Fe \rangle, Mgb)$ triplets. Diamonds, triangles, and squares refer to the most probable solution for each triplet, while crosses indicate the average of the logarithmic values of the solutions.

$$\alpha_\mu = \frac{\iiint_{G^*} \alpha P(t, Z, \alpha) dt dZ d\alpha}{\iiint_{G^*} P(t, Z, \alpha) dt dZ d\alpha}.$$

More specifically, we consider the subspace of solutions obtained with $f=0.9$. The uncertainties on the solutions are computed considering the whole G space:

$$\begin{aligned} \sigma_t^2 &= \frac{\iiint_G (t - t_\mu)^2 P(t, Z, \alpha) dt dZ d\alpha}{\iiint_G P(t, Z, \alpha) dt dZ d\alpha} \\ \sigma_Z^2 &= \frac{\iiint_G (Z - Z_\mu)^2 P(t, Z, \alpha) dt dZ d\alpha}{\iiint_G P(t, Z, \alpha) dt dZ d\alpha} \\ \sigma_\alpha^2 &= \frac{\iiint_G (\alpha - \alpha_\mu)^2 P(t, Z, \alpha) dt dZ d\alpha}{\iiint_G P(t, Z, \alpha) dt dZ d\alpha}. \end{aligned} \quad (28)$$

The analysis, repeated for the triplets $(H\beta, \langle Fe \rangle, Mgb)$, $(H\gamma_F, \langle Fe \rangle, Mgb)$, and $(H\delta_F, \langle Fe \rangle, Mgb)$, provides three different partial solutions, $t_{\mu,i}, Z_{\mu,i}$, and $\alpha_{\mu,i}$ for $i=1, 3$, with the corresponding uncertainties.

At this point we compare the results provided by the different index triplets and check for consistency within the errors. We observe that for those galaxies with low

or absent emission ($|EW_{em}(H\beta)| \leq 0.2$), there is a good agreement among the stellar population parameters derived with the use of the three different Balmer indices. For larger emissions, the results obtained with the $H\beta$ index deviate from the $H\gamma$ and $H\delta$ predictions however, with a tendency toward younger ages. Finally, for strong emissions ($|EW_{em}(H\beta)| > 0.6$), the infilling of the $H\gamma$ starts to become significant and the index, which has not been corrected for this effect, systematically provides very old ages. In this last case, the $H\delta$ index, that presents the lowest emission contamination, is perhaps the most reliable one. Thus we combine the information from the different index triplets, performing a weighted mean over those N indices which, according to the galaxy emission properties, provide a reliable solution as explained above:

$$t_f = \frac{\sum_{i=1}^N t_{\mu,i} W_{t,i}}{\sum_{i=1}^N W_{t,i}}; Z_f = \frac{\sum_{i=1}^N Z_{\mu,i} W_{Z,i}}{\sum_{i=1}^N W_{Z,i}}; \alpha_f = \frac{\sum_{i=1}^N \alpha_{\mu,i} W_{\alpha,i}}{\sum_{i=1}^N W_{\alpha,i}}, \quad (29)$$

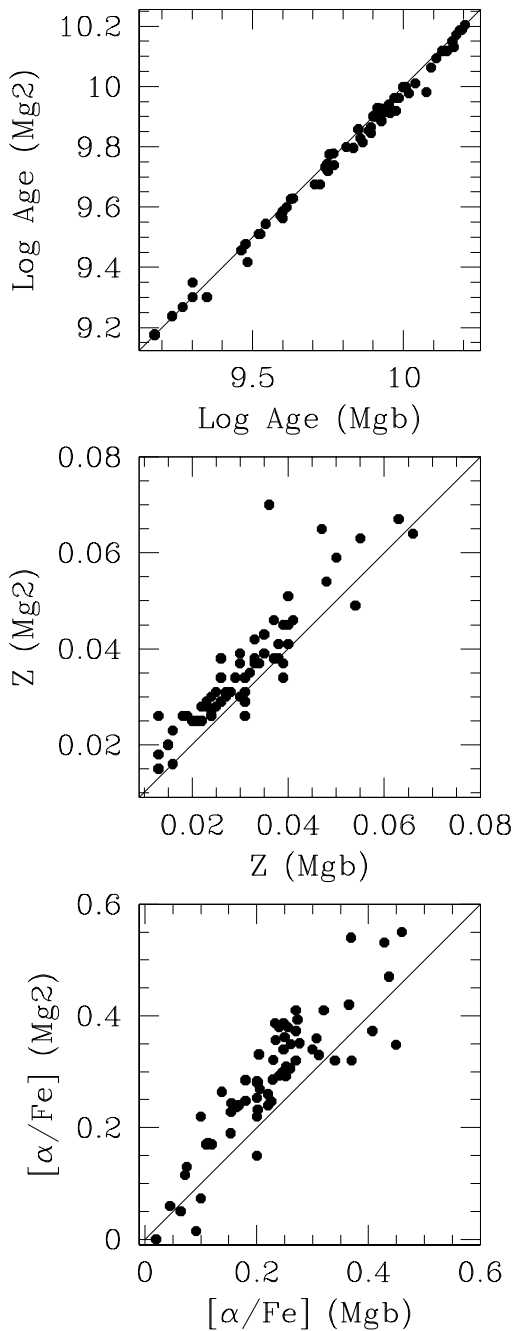


Fig. 10. Comparison of age, metallicity, and α -enhancement values derived using Mg2 instead of Mgb index.

where the weights are derived from the uncertainties on the parameters:

$$W_{t,i} = \frac{1}{\sigma_{t,i}^2}; W_{Z,i} = \frac{1}{\sigma_{Z,i}^2}; W_{\alpha,i} = \frac{1}{\sigma_{\alpha,i}^2}. \quad (30)$$

5. Stellar populations in early-type galaxies

Through the procedure described in Sect. 4.2, we have derived stellar population parameters (age, metallicity, and $[\alpha/\text{Fe}]$ ratio) for the apertures and gradients of the 62 galaxies plotted in Fig. 8. At the base of our analysis is the assumption that early-type galaxies contain almost co-eval stellar populations and may be well described by only one SSP. This is the most direct method to derive hints about the correlations between stellar population parameters and galaxy properties, like mass and environment. In the following analysis, we will focus both on the correlation between central galaxy populations and velocity dispersion/environment and on the analysis of the radial gradients.

5.1. Ages, metallicities, and α/Fe in the central region

We provide ages, metallicities, and $[\alpha/\text{Fe}]$ ratios derived from the three G-spaces ($\text{H}\beta$, $\langle \text{Fe} \rangle$, Mgb), ($\text{H}\gamma_F$, $\langle \text{Fe} \rangle$, Mgb), and ($\text{H}\delta_F$, $\langle \text{Fe} \rangle$, Mgb) for the apertures of the sample in Table 5 to 7. Column (1) gives the galaxy identification name, Col. (2) the aperture number (see Papers I and II for the aperture radii), and Cols. (3), (4), and (5) provide the age, the metallicity mass fraction Z ($Z = 0.018$ is the solar value) and the $[\alpha/\text{Fe}]$ ratio respectively. The complete tables are given in electronic form. In Table 8 we provide the final combined solutions for a $r_e/8$ aperture, obtained through Eqs. (26) and (27). Columns (1) and (2) give the galaxy identification name and the central velocity dispersion respectively. Columns (3), (4), and (5) provide the age, the metallicity mass fraction Z ($Z = 0.018$ is the solar value), and the $[\alpha/\text{Fe}]$ ratio, respectively.

Before continuing the discussion, we remark that our results are fairly independent of the choice of either magnesium index. Figure 10 compares the results obtained using the Mg2 index instead of the Mgb index. We notice a very good consistency in the derived ages, while the metallicity and α -enhancement would be only slightly higher adopting Mg2 instead of Mgb. However, the size of the latter differences will not affect our conclusions.

The distributions of age, metallicity, and enhancement within $r_e/8$ are shown in Figure 11. In each panel, we present the results obtained from the three different G spaces. We plot both the distributions for the total sample and the partial distributions for lenticular and elliptical galaxies. For all three index triplets, the age distribution shows a large spread (1 Gyr $<$ age $<$ 15 Gyr). From the $\text{H}\beta$ and $\text{H}\gamma$ indices, a bimodality, with a group of old objects (ages ≥ 7 Gyr), mainly composed by ellipticals, and a tail of young objects, mainly lenticulars, appears. We also observe that $\text{H}\beta$ tends to provide a larger number of very young galaxies than $\text{H}\gamma$ and $\text{H}\delta$. This effect is likely the result of the high uncertainty in the applied emission correction. However, we stress again that the method we adopted to combine the results from the different indices (see Sect. 4.2) allows us to clean our sample from spurious effect and obtain unbiased results for the final ages,

metallicities, and $[\alpha/\text{Fe}]$ ratios. The average ages for the whole sample, E and S0 obtained by properly combining the information from the three index triplets, are 8, 8.7, and 6.3 Gyr, respectively.

The metallicity distribution shows a broad peak, located between $0 < [\text{Z}/\text{H}] < 0.3$. There is a good agreement among the values derived from the analysis of the different index triplets, with the $\text{H}\delta$ distribution being peaked at slightly lower metallicities, which is an evident effect of the age-metallicity degeneracy. The average metallicities for the whole sample, E and S0, are 0.21, 0.22, and 0.19, respectively. Finally, the $[\alpha/\text{Fe}]$ ratio presents a maximum at ~ 0.22 with a narrower distribution than those of age and metallicity. The average ratios for the whole sample, E and S0, are 0.21, 0.23, and 0.17, respectively.

5.1.1. Correlation with central velocity dispersion

Figure 12 shows selected Lick indices measured in the central aperture ($r < r_e/8$) for the 65 galaxies of our sample as a function of central velocity dispersion. We observe that the separation between the two classes (those galaxies classified as E according to RC3 and those classified as S0) is quite well marked in velocity dispersion, with very few E galaxies populating the region below $\sigma_c \sim 180$ km/s. The fit to the total sample with coefficients is given in the upper label. We also show the percentage index variation along the regression when the velocity dispersion changes from $\sigma_c = 300$ km/s to $\sigma_c = 100$ km/s. Separate fits are made for the S0 and E galaxies.

It is clear that metallic indices show a well-established positive trend with σ_c (with a significantly shallower variation for the Fe indices). On the contrary, Balmer indices decrease with velocity dispersion. The observed behavior suggests metallicities or ages increasing with galaxy mass, but for the quantitative results we refer to the following comparison with SSP models.

To seek for possible correlation of the derived stellar population parameters with central velocity dispersion/galaxy mass, we plot the final solutions derived within a $r_e/8$ aperture (see Table 8) as function of σ_c in Fig. 13. In the top, central, and bottom panels, we plot ages, metallicities, and $[\alpha/\text{Fe}]$ ratios, respectively. Figure 13 shows a trend of increasing age with central velocity dispersion. Considering the separate fits for ellipticals and lenticulars, we obtain that the trend is positive for lenticulars and negative for ellipticals. However, a Spearman rank order test provides no proof for the existence of a correlation between age and $\sigma_c \simeq$ for both the whole sample and the E and S0 subsamples. The separate fits suggest that on average lenticulars are younger than ellipticals. The former, however, shows a large scatter. There is also a group of young E galaxies that deviate significantly from the main trend, at $\sigma_c \simeq 250$ km s $^{-1}$. The middle panel shows that there is a significant positive trend of metallicity with σ_c , with no significant difference in the slope between the two morphological types.

However, lenticular galaxies appear on average more metal rich than ellipticals at the same velocity dispersion. A Spearman test provides p-levels of significance¹ of 0.0001, 0.0002, and 0.07 for the whole sample, E and S0, respectively, confirming that there is strong correlation between the parameters. The same result is found for the α -enhancement, which again increases with central velocity dispersion. For the whole sample, the Spearman test results in a p level of 0.0008. The absence of a clear trend of age with σ_c , and the presence of strong correlations for metallicities and α -enhancement suggest that the galaxy gravitational potential must mainly affect the chemical enrichment process of the galaxy.

5.1.2. Correlation with environment

A measure of the richness of the environment, ρ_{xyz} , surrounding each galaxy in galaxies Mpc $^{-3}$, is reported by Tully (1988) for 47 galaxies (73% of the whole sample) (see Table 1). Even though our sample is prevalently made of field galaxies and we are far from the densities found in rich galaxy clusters, we may investigate how (eventually) the environment affects the trend of the physical parameters with velocity dispersion. In Fig. 14, we plot the derived age, metallicity, and enhancement values within an $r_e/8$ aperture as a function of the richness parameter ρ_{xyz} . Analogously to Fig. 13, E and S0 galaxies are denoted, and a linear fit is performed for all the galaxies and for the E and S0 subsamples. The upper panel indicates a positive trend of age with the richness parameter (the Spearman test provides a 85 % probability for a correlation to exist). As for what concerns metallicity and α -enhancement, there are no clear relations with ρ . The fitted relations to the data suggest that galaxies in lower density environments are slightly more metal rich and less enhanced in α -elements than galaxies in richer environments. However, a Spearman test does not provide any evidence for the existence of significant correlations.

The relation of age with environment is particularly interesting, in view of the fact that we have not found any trend with velocity dispersion. It is surprising that, in spite of containing more than 40% of the sample with determined ρ_{xyz} , the region above $\log(\rho_{xyz}) \geq -0.4$ does not contain galaxies younger than 4 Gyr. If we consider only galaxies with ages older than 4 Gyr, the resulting fit is flat, indicating that the age–environment relation is actually due to the presence of very young objects in the poorer environments. In fact, in such environments we have the contemporary presence of objects with both high and low velocity dispersions. It is also clear, after comparison with Fig. 13, that the clump of young E galaxies at $\sigma_c \simeq 250$ km s $^{-1}$ is due to objects located in a very low density environment.

Figure 14 also suggests that the relation with velocity dispersion may be "disturbed" by the presence of such ob-

¹ The p level of significance represents the probability that the relation found between the variables is not true.

Table 8. Average ages, metallicities, and α/Fe ratios ($r_e/8$ aperture)

Ident.	σ_c km s $^{-1}$	Age Gyr	Z	[α/Fe]
NGC 128	183	9.7 \pm 1.7	0.024 \pm 0.004	0.16 \pm 0.03
NGC 777	317	5.4 \pm 2.1	0.045 \pm 0.020	0.28 \pm 0.10
NGC 1052	215	14.5 \pm 4.2	0.032 \pm 0.007	0.34 \pm 0.05
NGC 1209	240	4.8 \pm 0.9	0.051 \pm 0.012	0.14 \pm 0.02
NGC 1297	115	15.5 \pm 1.2	0.012 \pm 0.001	0.29 \pm 0.04
NGC 1366	120	5.9 \pm 1.	0.024 \pm 0.004	0.08 \pm 0.03
NGC 1380	240	4.4 \pm 0.7	0.038 \pm 0.006	0.24 \pm 0.02
NGC 1389	139	4.5 \pm 0.6	0.032 \pm 0.005	0.08 \pm 0.02
NGC 1407	286	8.8 \pm 1.5	0.033 \pm 0.005	0.32 \pm 0.03
NGC 1426	162	9.0 \pm 2.5	0.024 \pm 0.005	0.07 \pm 0.05
NGC 1453	289	9.4 \pm 2.1	0.033 \pm 0.007	0.22 \pm 0.03
NGC 1521	235	3.2 \pm 0.4	0.037 \pm 0.006	0.09 \pm 0.02
NGC 1533	174	11.9 \pm 6.9	0.023 \pm 0.020	0.21 \pm 0.10
NGC 1553	180	4.8 \pm 0.7	0.031 \pm 0.004	0.10 \pm 0.02
NGC 1947	142	5.9 \pm 0.8	0.023 \pm 0.003	0.05 \pm 0.02
NGC 2749	248	10.8 \pm 2.3	0.027 \pm 0.006	0.25 \pm 0.04
NGC 2911	235	5.7 \pm 2.0	0.034 \pm 0.019	0.25 \pm 0.10
NGC 2974	220	13.9 \pm 3.6	0.021 \pm 0.005	0.23 \pm 0.06
NGC 3136	230	1.5 \pm 0.1	0.089 \pm 0.004	0.36 \pm 0.02
NGC 3258	271	4.5 \pm 0.8	0.047 \pm 0.013	0.21 \pm 0.03
NGC 3268	227	9.8 \pm 1.7	0.023 \pm 0.004	0.34 \pm 0.04
NGC 3489	129	1.7 \pm 0.1	0.034 \pm 0.004	0.05 \pm 0.02
NGC 3557	265	5.8 \pm 0.8	0.034 \pm 0.004	0.17 \pm 0.02
NGC 3607	220	3.1 \pm 0.5	0.047 \pm 0.012	0.24 \pm 0.03
NGC 3818	191	8.8 \pm 1.2	0.024 \pm 0.003	0.25 \pm 0.03
NGC 3962	225	10.0 \pm 1.2	0.024 \pm 0.003	0.22 \pm 0.03
NGC 4374	282	9.8 \pm 3.4	0.025 \pm 0.010	0.24 \pm 0.08
NGC 4552	264	6.0 \pm 1.4	0.043 \pm 0.012	0.21 \pm 0.03
NGC 4636	209	13.5 \pm 3.6	0.023 \pm 0.006	0.29 \pm 0.06
NGC 4696	254	16.0 \pm 4.5	0.014 \pm 0.004	0.30 \pm 0.10
NGC 4697	174	10.0 \pm 1.4	0.016 \pm 0.002	0.14 \pm 0.04
NGC 5011	249	7.2 \pm 1.9	0.025 \pm 0.008	0.25 \pm 0.06
NGC 5044	239	14.2 \pm 10.	0.015 \pm 0.022	0.34 \pm 0.17
NGC 5077	260	15.0 \pm 4.6	0.024 \pm 0.007	0.18 \pm 0.06
NGC 5090	269	10.0 \pm 1.7	0.028 \pm 0.005	0.26 \pm 0.04
NGC 5193	209	6.8 \pm 1.1	0.018 \pm 0.002	0.26 \pm 0.04
NGC 5266	199	7.4 \pm 1.4	0.019 \pm 0.003	0.15 \pm 0.05
NGC 5328	303	12.4 \pm 3.7	0.027 \pm 0.006	0.15 \pm 0.05
NGC 5363	199	12.1 \pm 2.3	0.020 \pm 0.004	0.16 \pm 0.05
NGC 5638	168	9.1 \pm 2.3	0.024 \pm 0.008	0.24 \pm 0.05
NGC 5812	200	8.5 \pm 2.1	0.027 \pm 0.008	0.22 \pm 0.05
NGC 5813	239	11.7 \pm 1.6	0.018 \pm 0.002	0.26 \pm 0.04
NGC 5831	164	8.8 \pm 3.5	0.016 \pm 0.011	0.21 \pm 0.09
NGC 5846	250	8.4 \pm 1.3	0.033 \pm 0.005	0.25 \pm 0.03
NGC 5898	220	7.7 \pm 1.3	0.030 \pm 0.004	0.10 \pm 0.03
NGC 6721	262	5.0 \pm 0.8	0.040 \pm 0.007	0.24 \pm 0.02
NGC 6758	242	16.0 \pm 2.5	0.016 \pm 0.002	0.32 \pm 0.05
NGC 6776	242	2.7 \pm 0.5	0.033 \pm 0.010	0.21 \pm 0.05
NGC 6868	277	9.2 \pm 1.8	0.033 \pm 0.006	0.19 \pm 0.03
NGC 6876	230	9.8 \pm 1.6	0.023 \pm 0.003	0.26 \pm 0.03
NGC 6958	223	3.0 \pm 0.3	0.038 \pm 0.006	0.20 \pm 0.03
NGC 7007	125	3.4 \pm 0.6	0.031 \pm 0.010	0.15 \pm 0.05
NGC 7079	155	6.7 \pm 1.1	0.016 \pm 0.003	0.21 \pm 0.05
NGC 7097	224	10.5 \pm 2.4	0.024 \pm 0.005	0.30 \pm 0.05
NGC 7135	231	2.2 \pm 0.4	0.047 \pm 0.010	0.46 \pm 0.04
NGC 7192	257	5.7 \pm 2.0	0.039 \pm 0.015	0.09 \pm 0.05
NGC 7332	136	3.7 \pm 0.4	0.019 \pm 0.002	0.10 \pm 0.03
NGC 7377	145	4.8 \pm 0.6	0.020 \pm 0.002	0.10 \pm 0.03

!

Table 8 Continue. Average ages, metallicities, and α/Fe ratios ($r_e/8$ aperture)

Ident.	σ_c km s $^{-1}$	Age Gyr	Z	[α/Fe]
IC1459	311	8.0 ± 2.2	0.042 ± 0.009	0.25 ± 0.04
IC2006	122	8.1 ± 0.9	0.026 ± 0.003	0.12 ± 0.02
IC3370	202	5.6 ± 0.9	0.022 ± 0.004	0.17 ± 0.04
IC4296	340	5.2 ± 1.0	0.044 ± 0.008	0.25 ± 0.02

Notes: the values are obtained combining the $\text{H}\beta$, $\text{H}\gamma$, $\text{H}\delta$, Mgb , and $\langle \text{Fe} \rangle$ indices as described in Sect. 4.2.

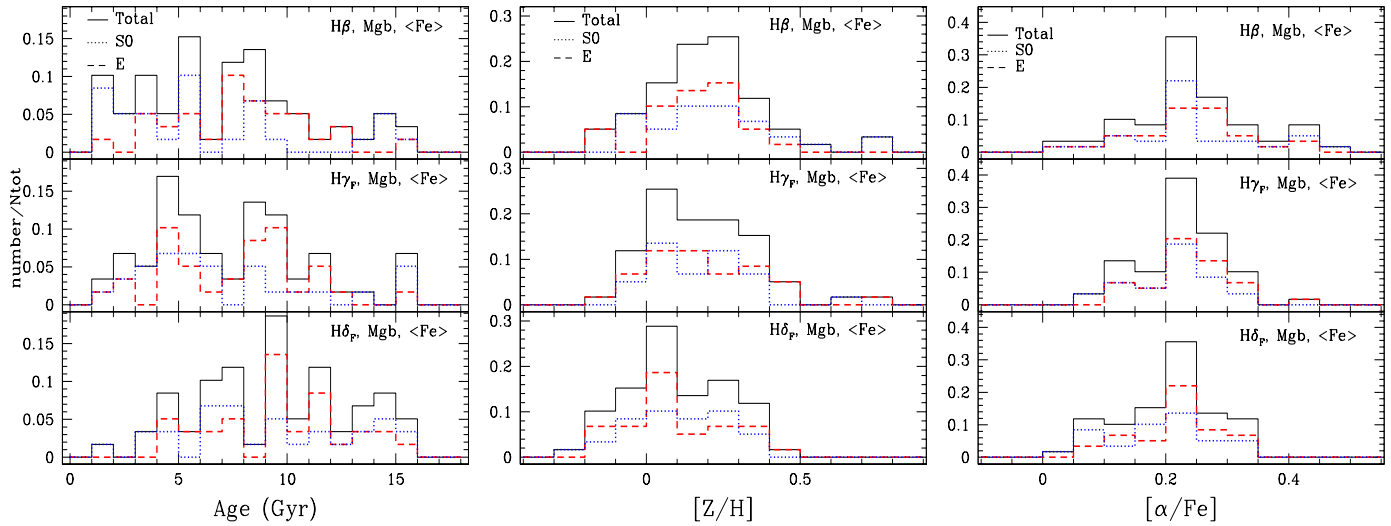


Fig. 11. Distribution of ages (left panel), metallicities (central), and $[\alpha/\text{Fe}]$ ratios (right) measured at $r_e/8$, derived from the $(\text{H}\beta, \langle \text{Fe} \rangle, \text{Mgb})$, $(\text{H}\gamma_F, \langle \text{Fe} \rangle, \text{Mgb})$, and $(\text{H}\delta_F, \langle \text{Fe} \rangle, \text{Mgb})$ index spaces. In the plot we have included only the galaxies for which the solution is derived within 1σ from the observed indices. The solid line refers to the total sample, while the dotted and dashed lines are for S0s and Es, respectively. For each distribution, the used index triplet is provided in the label inside the box.

jects populating very low density environments. In Fig. 15, we have redrawn the fit with velocity dispersion separating objects according to their richness parameter, instead of morphological type. A linear fit is performed for all the galaxies, while fits to the galaxies in high and low density environments are also performed separately. We notice that at values $\log(\rho_{xyz}) \approx -0.4$, we may identify small associations of galaxies, such as pairs and poor galaxy groups, in the Tully (1988) catalogue. On the upper side, above $\log(\rho_{xyz}) \approx 0.0$ typical of the outskirts of Virgo cluster, we count only four objects, and we stress again that our *rich environment* is not representative of rich clusters. Again there is no clear trend of age with velocity dispersion, but now galaxies in relatively richer environments are more tightly clustered around the average relation. The following correlations are derived for age, metallicity, and α/Fe enhancement, respectively:

$$\begin{aligned} \text{Log(age/Gyr)} &= -0.15 + 0.43 \times \log(\sigma_c) & (\text{Total : } r = 0.2) \\ \text{Log(age/Gyr)} &= -0.51 + 0.56 \times \log(\sigma_c) & (\text{LDE : } r = 0.24) \\ \text{Log(age/Gyr)} &= 0.86 + 0.03 \times \log(\sigma_c) & (\text{HDE : } r = 0.01) \end{aligned} \quad (31)$$

$$\begin{aligned} \text{Log}(Z/Z_\odot) &= -0.99 + 0.48 \times \log(\sigma_c) & (\text{Total : } r = 0.34) \\ \text{Log}(Z/Z_\odot) &= -0.85 + 0.44 \times \log(\sigma_c) & (\text{LDE : } r = 0.3) \\ \text{Log}(Z/Z_\odot) &= -1.36 + 0.64 \times \log(\sigma_c) & (\text{HDE : } r = 0.47) \end{aligned} \quad (32)$$

$$\begin{aligned} [\alpha/\text{Fe}] &= -0.74 + 0.41 \times \log(\sigma_c) & (\text{Total : } r = 0.53) \\ [\alpha/\text{Fe}] &= -0.79 + 0.43 \times \log(\sigma_c) & (\text{LDE : } r = 0.52) \end{aligned}$$

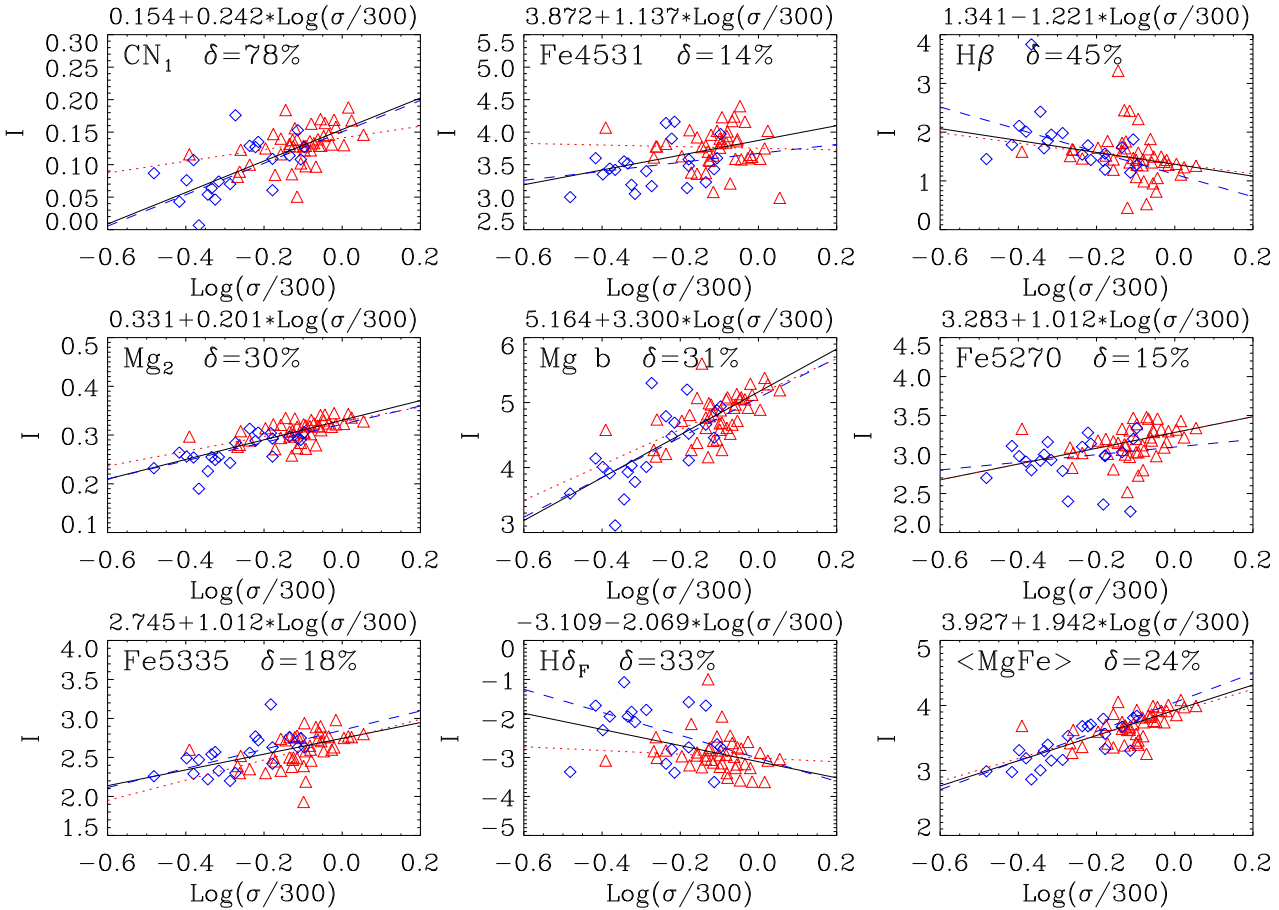


Fig. 12. Selected Lick indices, measured at $r < r_e/8$, for the total sample of 65 galaxies as a function of $\log(\sigma_c/300)$, where σ_c is the central velocity dispersion. Triangles and diamonds indicate E and S0 galaxies, respectively. The dashed, dotted, and solid lines mark the linear fit obtained for S0 galaxies, E galaxies, and the total sample, respectively. For each index, the linear fit to the total sample is labeled above each panel.

$$[\alpha/\text{Fe}] = -0.87 + 0.47 \times \log(\sigma_c) \quad (\text{HDE : } r = 0.58), \quad (33)$$

where LDE and HDE indicate galaxies populating low and high density regions, respectively, and r is the linear correlation coefficient.

At 200 km s^{-1} , the average age of galaxies inhabiting HDE is of about 8.5 Gyr, while those in LDE is $\simeq 6$ Gyr. As far as the relation between metallicity and σ_c is concerned, we notice that there is almost no dependence on the environment. The different relations are almost superimposed, with the only noticeable difference being that the galaxies in HDE are less dispersed than those in LDE. The same is valid for the enhancement.

Summarizing, combining the information of Fig. 15 with the behavior of the stellar population parameters with environment, we argue that the metal enrichment is essentially dominated by the gravitational binding of the parent galaxy. In reverse, the way in which the populations are assembled (the growth of baryons within galaxies) seems modulated by the environment, with galaxies in richer environments being on average older than galaxies

in less rich environments. Galaxies in more rich environments show a lack of very young members. Since environment seems to have no effect on the metallicity- σ_c and $[\alpha/\text{Fe}]-\sigma_c$ relations, we argue that very young members in the lowest density regions are more likely due to rejuvenation episodes than to more prolonged star formations.

5.2. Stellar population gradients

Gradients within galaxies can provide further insight on the process of formation and evolution of early-type galaxies. Our sample shows the presence of clear gradients in the observed line-strength indices. Gradients have been extracted from a linear fit to the index values measured in the four radial regions $0 \leq r \leq r_e/16$, $r_e/16 \leq r \leq r_e/8$, $r_e/8 \leq r \leq r_e/4$, and $r_e/4 \leq r \leq r_e/2$.

In Fig. 16 we show as an example the observed index gradients as a function of σ_c for some selected indices. Analogously to Fig. 13, we have used different symbols for S0 and E galaxies, and different lines to denote the fits to S0 and E separately, and the fit to the total sample. The figure, besides showing the presence of eventual gradients of indices, highlights whether a corre-

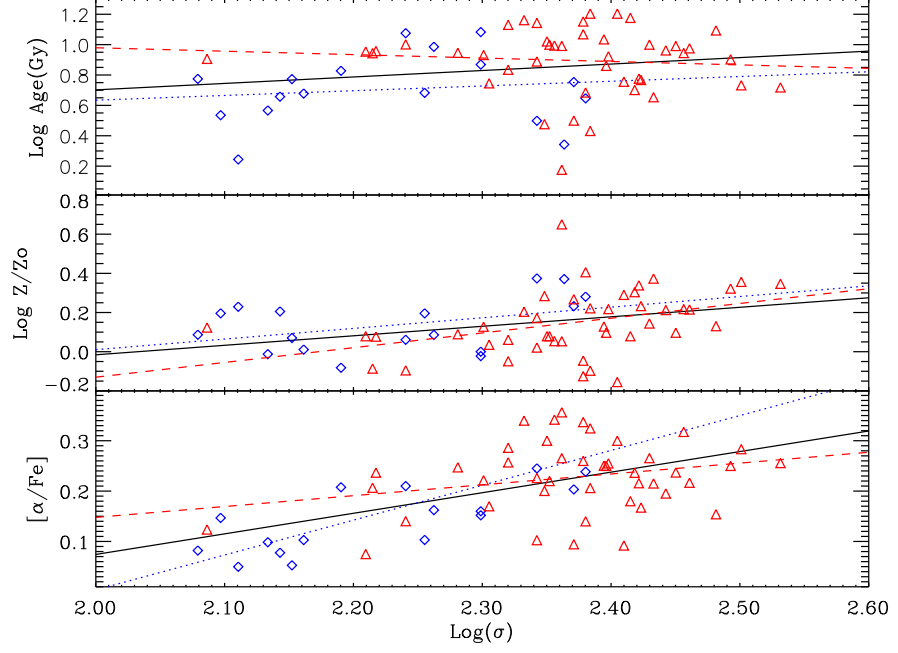


Fig. 13. Ages, metallicities, and $[\alpha/\text{Fe}]$ ratios, measured at $r_e/8$, vs. the central velocity dispersion, $\log \sigma_c$. The plotted stellar population parameters are derived from the combined analysis of the $(\text{H}\beta, \langle \text{Fe} \rangle, \text{Mgb})$, $(\text{H}\gamma_F, \langle \text{Fe} \rangle, \text{Mgb})$, and $(\text{H}\delta_F, \langle \text{Fe} \rangle, \text{Mgb})$ index spaces (see text for details). Triangles and diamonds denote, respectively, E and S0 galaxies. The solid line is the linear fit performed to all the galaxies, while dashed and dotted lines are the best fit to Es and S0s subsamples.

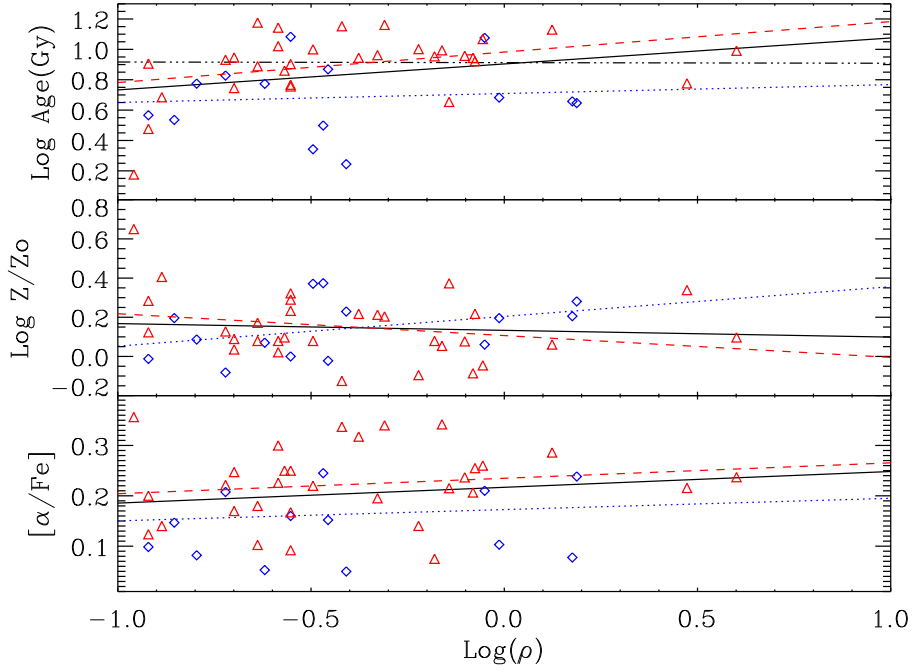


Fig. 14. Ages, metallicities, and $[\alpha/\text{Fe}]$ ratios, measured at $r_e/8$, vs. the density of the environment, $\log(\rho)$, in galaxies Mpc^{-3} (Tully 1988, see Table 1). Triangles and diamonds denote, respectively, E and S0 galaxies. The solid line is the linear fit performed to all the galaxies. Dashed and dotted lines are the best fit to E and S0 subsamples. The dot-dashed line is the fit for the galaxies older than 4 Gyr.

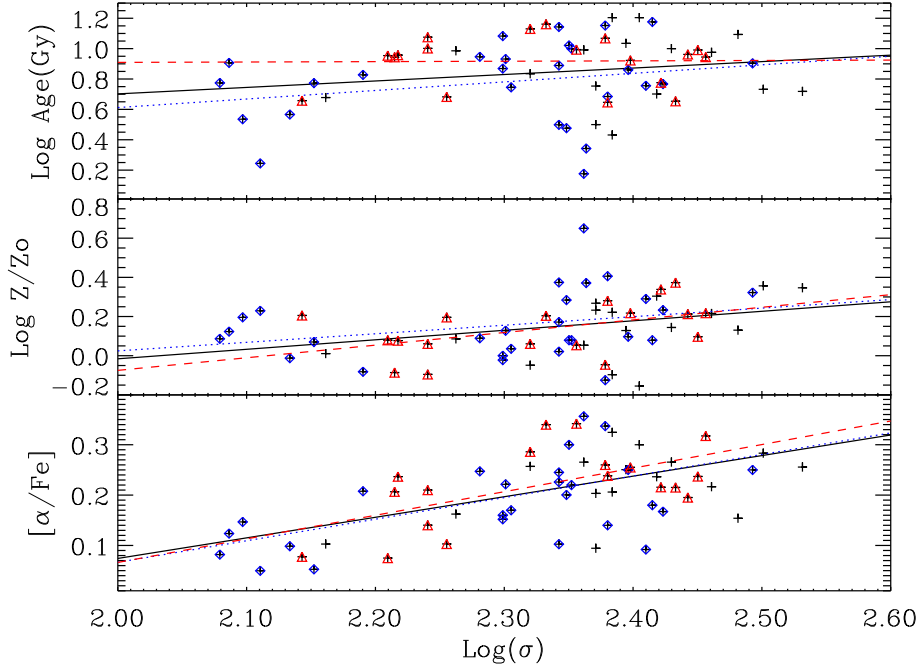


Fig. 15. Ages, metallicities, and $[\alpha/\text{Fe}]$ ratios, measured at $r_e/8$, vs. the central velocity dispersion, $\log \sigma_c$. In this figure triangles denote galaxies with a relatively higher richness parameter, $\log(\rho) \geq 0.4$. Diamonds denote the other objects, while crosses denote the total sample. The solid line is the linear fit performed to all the galaxies. The dashed and the dotted lines refer to galaxies in high and low density environments, respectively.

lation between the gradient and the gravitational potential of the galaxy exists. From Fig. 16, we notice that in general metallic indices decrease from the center of the galaxy outwards, while Balmer indices (i.e., $\text{H}\beta$, $\text{H}\delta$) increase. Such a behavior suggests that either metallicity or age decreases from the central regions of the galaxy to the periphery. As far as the modulation of the gradients with velocity dispersion is concerned, we notice that larger gradients tend to correspond to lower σ_c values (at least for the metallic indices), suggesting that stellar population gradients tend to flatten with increasing galaxy mass. However, these are only qualitative conclusions, and the quantitative derivation of the stellar population gradients requires the comparison of the observed indices with SSP models. Age, metallicity, and $[\alpha/\text{Fe}]$ values derived for the gradients ($0 < r < r_e/16$, $r_e/16 < r < r_e/8$, $r_e/8 < r < r_e/4$, $r_e/4 < r < r_e/2$) are provided for the three G-spaces ($\text{H}\beta$, $\langle \text{Fe} \rangle$, Mgb), ($\text{H}\gamma_F$, $\langle \text{Fe} \rangle$, Mgb), and ($\text{H}\delta_F$, $\langle \text{Fe} \rangle$, Mgb) and for the final solution (Eq. 29) in Tables 9 to 12. The complete tables are given in electronic form. For a more detailed presentation of the results with complete figures for the stellar population gradients, we refer to Annibali (2005). Gradients are expressed as $\delta \log(\text{Age}/\text{Gyr})/\delta \log(r/r_e)$, $\delta \log(Z)/\delta \log(r/r_e)$, and $\delta[\alpha/\text{Fe}]/\delta \log(r/r_e)$, respectively.

We plot the distributions of age, metallicity, and α -enhancement gradients in Fig. 17. The age and $[\alpha/\text{Fe}]$ gradients present a large dispersion. The age gradients are

symmetrically distributed around zero, while the $[\alpha/\text{Fe}]$ gradients show a low peak at negative values. The metallicity gradient distribution is the only one that presents a clear peak at negative values. We derive an average metallicity gradient of -0.21.

As was done for the stellar population parameters derived within a $r_e/8$ aperture, we investigate possible trends of the gradients with the richness parameter ρ (Fig. 18) and the central velocity dispersion (Fig. 19). In Fig. 18 E and S0 galaxies are denoted. A linear fit is performed for all the galaxies, and fits are also performed for the E and S0 subsamples. Like in Figure 14, a fit to all the galaxies older than 4 Gyr is performed. We notice that for the gradients there is not the dichotomy, revealed by Fig. 14, between objects of relatively high and relatively low richness parameters. However, there are hints of the existence of trends in the gradients with the richness parameter. The most evident trends are revealed by the chemical enrichment path. The metallicity gradient is at values around -0.25 (in good agreement with, e.g., Davies et al. 1993), but seems to vanish at increasing richness. The tendency seems even more clear if only ellipticals are considered. The gradient of α -enhancement is slightly negative at very low density and increases with the richness parameter. The dispersion is, however, larger than in the case of the metallicity gradient, and, in spite of the trend suggested by the linear fits, according to a Spearman rank order test, there

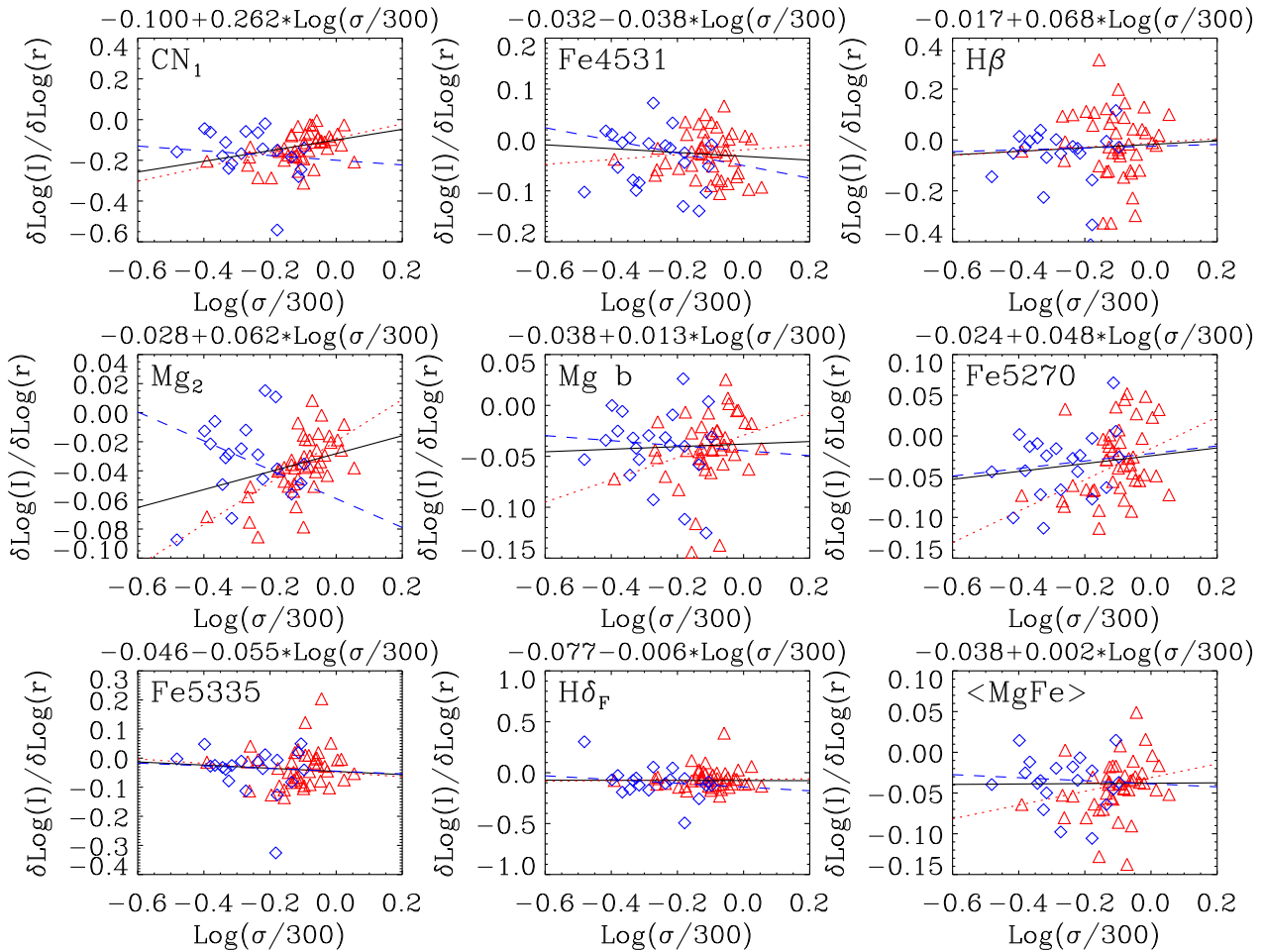


Fig. 16. Gradients of Lick indices computed as $\delta I/\delta \log(r)$ for the total sample of 65 galaxies as a function of $\log(\sigma_c/300)$, where σ_c is the central velocity dispersion. Triangles and diamonds denote, respectively, E and S0 galaxies. The dashed, dotted, and solid lines mark the linear fit obtained for S0 galaxies, E galaxies, and the total sample, respectively. For each index, the linear relation that fits the total sample is labeled above each panel.

is no significant correlation between the gradients and the density parameter ρ .

In Fig. 19 we consider the relation between gradients and central velocity dispersion once, as in Fig. 15, we have separated galaxies according to their richness parameter. There is no significant trend of the age gradient with velocity dispersion for the whole sample. Again, the most important trends are those of metallicity and α/Fe enhancement. For the whole sample, the metallicity gradient shows an increasing trend with velocity dispersion (larger negative gradients for less massive systems); a Spearman test provides a significance level of 0.07 (93% probability that a correlation exist). The correlation is very strong if only E galaxies are considered ($p = 0.009$). As for the $[\alpha/\text{Fe}]$ gradient, it is slightly positive and constant for HDE galaxies ($\delta[\alpha/\text{Fe}]/\delta \log(r/r_e) \sim 0.05$). LDE galaxies have preferentially negative gradients, with all galaxies above 200 km/s lying below the relation defined by HDE galaxies. There are essentially no differences if we considered the sample of E and S0 galaxies separately (the plot is not shown here).

6. Discussion

How and when early-type galaxies formed is still a matter of debate. Two alternative formation scenarios have been proposed in the past. In the monolithic one, the spheroidal component forms by the gravitational collapse of a gas cloud with considerable energy dissipation (Larson 1974b; Arimoto & Yoshii 1987). As a result of the rapidity of this collapse, the bulk of stars in ellipticals should be relatively old. Unfortunately, this scenario is not supported by detailed hydrodynamical calculations: any angular momentum initially present in the overdensity region prevents the rapid collapse of the gas. Small disk-like entities are formed first, and only after subsequent major merging events may they give rise to the spheroidal component of the galaxies (Toomre 1977; Kauffmann et al. 1993; Baugh, Cole & Frenk 1996; Steinmetz & Navarro 2002). The star formation process is delayed in this so-called hierarchical scenario, which then predicts the presence of significant intermediate-age stellar populations.

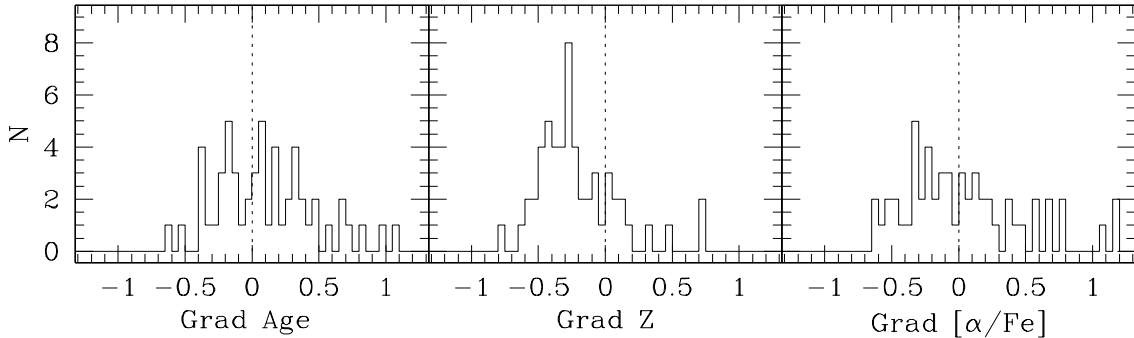


Fig. 17. Distributions of the age, metallicity, and $[\alpha/\text{Fe}]$ gradients computed as $\delta \log(\text{Age}/\text{Gyr})/\delta \log(r/r_e)$, $\delta \log(\text{Z})/\delta \log(r/r_e)$, and $\delta [\alpha/\text{Fe}]/\delta \log(r/r_e)$, respectively. The dotted vertical line separates negative from positive gradient values.

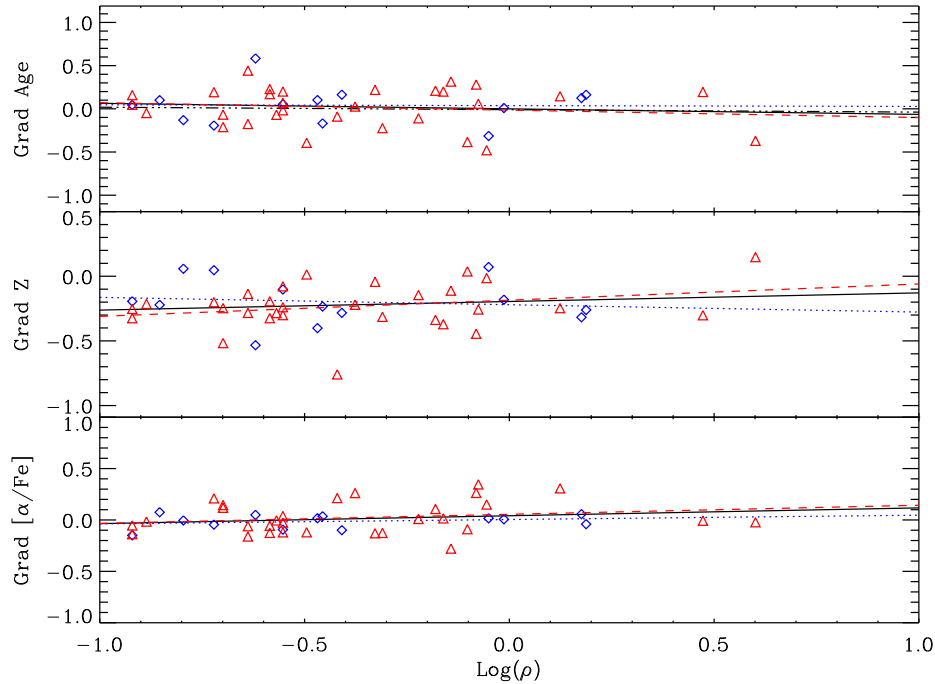


Fig. 18. Age, metallicity, and $[\alpha/\text{Fe}]$ gradients against the density parameter, $\log(\rho)$. Triangles and diamonds represent, respectively, E and S0 galaxies. The solid line is the linear best fit performed to all the galaxies. Dashed and dotted lines are the best fit to the E and S0 subsamples. The dot-dashed line best fits all galaxies older than 4 Gyr.

The study of absorption line indices in local early-type galaxies has proven to be one of the most powerful diagnostics to constrain star formation history and to trace star evolution over time. Besides "direct" age estimates, indirect evidences of the duration of the star formation process can be analyzed through the study of the chemical enrichment pattern, and more specifically of the α/Fe enhancement. While the α -elements O, Na, Mg, Si, S, Ar, Ca, and Ti (particles that are built up with α -particle nuclei) plus the elements N and Ne are derived mainly by Type II supernova explosions of massive progenitor stars, a substantial fraction of the Fe-peak elements Fe and

Cr comes from the delayed exploding Type Ia supernovae (Nomoto et al. 1984; Woosley & Weaver 1995; Thielemann et al. 1996). Hence, the α/Fe ratio quantifies the relative importance of Type II and Type Ia supernovae (Greggio & Renzini 1983; Matteucci & Greggio 1986; Pagel & Tautvaišienė 1995; Thomas et al. 1998), and therefore carries information about the timescale over which star formation occurs. Thus, the α/Fe ratio can be considered to be an additional robust measure of the duration of the star formation process. Finally, a great deal of information on the formation process comes nowadays from simulations that are able to predict the radial distribution of the stellar

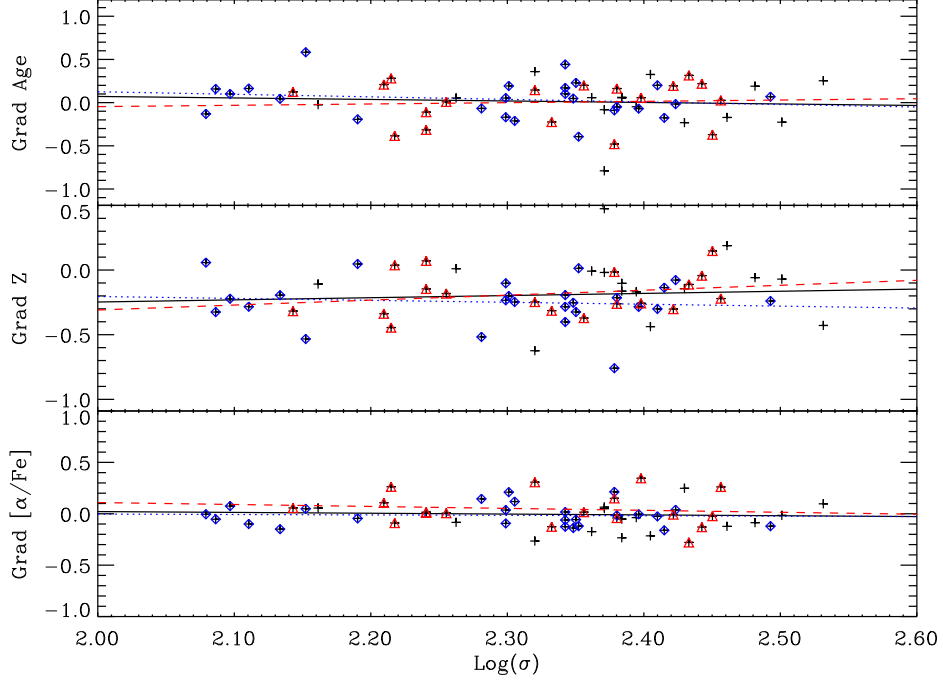


Fig. 19. Age, metallicity, and $[\alpha/\text{Fe}]$ gradients vs. the central velocity dispersion $\log \sigma_c$. The plotted stellar population parameters are derived from the combined analysis of the $(\text{H}\beta, \langle \text{Fe} \rangle, \text{Mgb})$, $(\text{H}\gamma_F, \langle \text{Fe} \rangle, \text{Mgb})$, and $(\text{H}\delta_F, \langle \text{Fe} \rangle, \text{Mgb})$ index spaces (see text for details). Triangles are galaxies with relatively high density parameter ($\log(\rho) \geq -0.4$), and diamonds the other objects, while crosses mark the whole sample. The solid line is the linear best fit performed to all the galaxies. The dashed and dotted lines are the best fits to the galaxies located in relatively high and low density environments, respectively.

populations within the galaxy (Larson 1974a; Larson 1975; Carlberg 1984; Bekki & Shioya 1999; Chiosi & Carraro 2002; Kawata & Gibson 2003; Kobayashi 2004). In the following we will summarize all the information we have deduced from the analysis of our sample, and see what scenario is more suited for early-type galaxies in low density environment.

6.1. The scaling relations for field early-type galaxies

An important result of our analysis is the derivation of correlations between the stellar population parameters and the galaxy potential well as a function of environment for our sample of galaxies. Other studies in the literature have presented scaling relations for early-type galaxies on the basis of different samples and/or stellar population models, among which the most recent are those of Thomas et al. (2005, T05), Denicoló et al. (2005b, D05), Gallazzi et al. (2005, G05) and Clemens et al. (2006, C06).

T05 have assembled three different data sets: G93, Beuing et al. (2002) and Mehrt et al. (2000, 2003). Their sample contains objects located in both "high" and "low" surface density environments. It is worth noticing that $\text{H}\beta$ emission corrections have been applied by G93 and by Mehrt et al. (2000, 2003) but not by Beuing et al. (2002). T05 generated mock catalogues starting from the

velocity dispersion distribution of the sample and assuming suitable scaling relations between the SSP parameters and the velocity dispersion (allowing for dispersion and for observational errors). The scaling relations are then modified until the best "by-eye" fit to the indices ($\text{H}\beta$, Mgb , and $\langle \text{Fe} \rangle$) is obtained.

D05 have derived ages, metallicities, and $[\alpha/\text{Fe}]$ ratios at $r_e/8$ for a sample of 83 early-type galaxies essentially in groups, the field, or isolated objects, which consist of 52 elliptical galaxies and 31 bulges of S0s or early-type spirals. Their results are based on the comparison of the measured $\text{H}\beta$, Mgb , Mg2 , $\langle \text{Fe} \rangle$ and $[\text{Mg}/\text{Fe}]$ indices with the TMB03 models. The $\text{H}\beta$ values used in their analysis were corrected for emission contamination through the $\text{H}\alpha$ line (see also Sect. 2 of this paper).

G05 presented stellar metallicities and ages for a magnitude limited sample of $\sim 26,000$ early-type galaxies drawn from the Sloan Digital Sky Survey Data Release Two (SDSS DR2). Their analysis rests on the recent population synthesis models of Bruzual & Charlot (2003) and is based on the simultaneous fit of five spectral absorption features (among which are $\text{H}\beta$ and $\text{H}\delta_A + \text{H}\gamma_A$), which depend only weakly on the α/Fe element abundance ratio. Before comparison with models, spectra were corrected for nebular emission lines. In their analysis $[\alpha/\text{Fe}]$ ratios have not been derived.

C06 have used the SSPs presented in this work to analyze a volume limited subsample of about 4000 early-type galaxies in the Third Release of SDSS catalogue. By considering 11 Lick indices at once, C06 have derived mean age, metallicity, and enhancement variations as a function of the dispersion velocity and environment.

When comparing our results with the above literature we should keep in mind that: **(a)** the simple stellar population models adopted are different (in particular TMB03 models are based on different stellar evolutionary tracks and on a different index dependence with element abundance with respect to our new models); **(b)** different line-strength indices are used in the analysis: in particular, while T05 and D05 adopt a single age indicator, the $H\beta$ index, G05, and this work are based on the use of multiple age indicators ($H\beta$, $H\delta$, and $H\gamma$), which allow us to minimize uncertainties due to emission contamination. Finally, C06 use a simultaneous least-square fit to 11 index derivatives that takes their age/metallicity/enhancement (and also $[C/Fe]$) sensitivity into account; **(c)** Our sample is biased not only towards early-type galaxies in LDE, but also towards galaxies whose spectra show emission lines, since we selected them to find ISM traces. T05 divide their sample into low and high density classes, but in both works the classification is performed on the basis of a subjective estimate of galaxy density (while we use density parameter, which is a properly measured volume density). The D05 sample contains galaxies biased toward low density environment and G05 and C06 samples are drawn from the SDSS, which contains galaxies belonging to a wide range of environments, but predominantly composed of galaxies in low density regions. Finally, D05 and G05 provide only qualitative trends of the derived stellar population parameters, while C06 provide differential variations as a function of velocity dispersion. In the following we will perform a detailed comparison of the results obtained in this work with those obtained in the above quoted papers. However, for the sake of conciseness, we will limit the graphical comparison of the scaling relations to the work of T05, while we will only quote the results obtained by the other authors.

6.1.1. The age scaling relation

In the top panel of Fig. 20, we compare the age scaling relations obtained by T05 for the galaxies in low density environments with our results for the total sample, for HDE galaxies and for LDE galaxies, respectively. It is worth noticing that the fit of T05 refers to a group of "passively" evolving galaxies (in the low density environment subsample) selected in the $H\beta$ -[MgFe] diagram, while we have selected, in our field sample, a subsample of "passively" evolving galaxies by considering a density threshold limit above which there is no evidence of rejuvenation episodes (see Sect. 5.1.2). Thus, when comparing to T05, we consider their scaling relations for the galaxies in a low density environment and our results for the

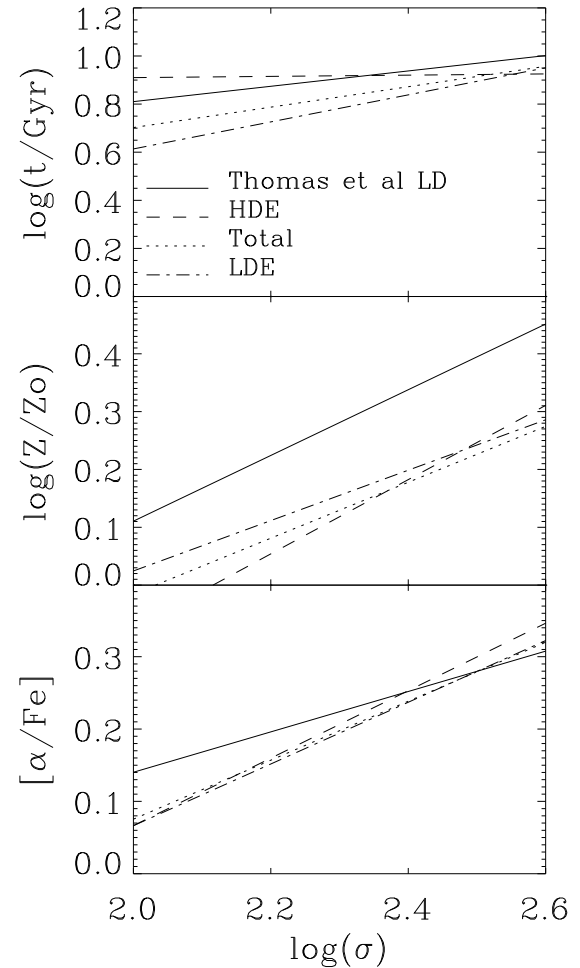


Fig. 20. Scaling relations obtained in this work compared with those of Thomas et al. (2005) for their low density environment galaxies. Solid lines refer to Thomas et al. (2005), while dashed, dot-dashed, and dotted lines refer to our HDE and LDE galaxies and to the total sample.

HDE. The most noticeable difference between the age- σ_c relation obtained in this work and that of T05 is in the slope. T05 find increasing ages with velocity dispersion (slope ~ 0.32), while we derive a flat relation (slope of ~ 0.03). However, we notice that the linear correlation coefficient is poor in both cases (Eq. (31)), indicating that the spread of the data around the relation is large, and, given the limited number of objects, the error on the coefficients is also large. We also notice that if we consider the whole HDE + LDE sample, where young galaxies are present, we get a positive trend with a slope of 0.43. However, as already discussed in Sect. 5.1.1, a Spearman rank order test does not provide significant correlation between age and velocity dispersion.

Our results are more consistent with those of G05 and C06. G05 do not find any significant variation of age with stellar mass (in their early-type sub-sample), except for a population of young metal-poor galaxies in the lowest mass bins. C06 find a significant flattening of the age above $\sigma \sim 170 \text{ km/s}$. D05 estimate an average age of 5.8 Gyr for

Es and 3 Gyr for S0s, with hints of a trend for massive galaxies to be older.

6.1.2. The metallicity scaling relation

The relation between metallicity and velocity dispersion is shown in the central right panel of Fig. 20. The slope we have derived (~ 0.64) falls between the one derived by T05 (~ 0.57) and that derived by C06 (0.76). However, there is a significant zero point offset between T05 and our relation, with the metallicity derived by T05 being about 0.15 dex larger than ours. At 100 km s^{-1} , T05 find an average metallicity for galaxies in low density environment that is 26% larger than solar. Instead, we find that at the same velocity dispersion the average metallicity of old field galaxies should be $\sim 80\%$ of the solar one. Our derived relation is in good agreement with metallicity estimates of stars of our own Bulge: the average metallicity of the Bulge is found to be $[\text{Fe}/\text{H}] \simeq -0.2$ (Ramirez et al. 2000; Mc William & Rich 1994) and, with its velocity dispersion of $\sigma_c \simeq 104 \text{ km s}^{-1}$ (Blum, 1995), it fall just slightly below our relation. The zero point offset is most likely caused by the different evolutionary tracks adopted as fully discussed in Sect. 3.

Apart from this offset, the estimate of the slope of the relation seems very robust, because it is quite independent from the adopted sample and from the analysis process. The linear correlation coefficient and the Spearman test indicate that the relation between metallicity and σ_c is fairly tight. If we add the additional evidence that the slope seems to be almost independent from the environment (Eq. (32) and T05), we may conclude that the metallicity- σ_c relation is perhaps witnessing one of the tightest links between stellar populations and structural parameters.

A metallicity increase with galaxy mass is found by D05 and G05 as well. However, the metallicities derived by D05 are larger when compared to our work and that of G05, likely because of the use of TMB03 models: at $\sigma \sim 300 \text{ km/s}$ D05 derive metallicities above 0.3 dex, while the G05 metallicities are peaked around $\log Z/Z_\odot \sim 0.15$ and our relation gives $\log Z/Z_\odot \sim 0.22$. We find only a slight dependence of the metallicity- σ relation on the richness parameter, in agreement with T05, while C06 find none, in their much larger sample.

6.1.3. The α -enhancement scaling relation

Our α -enhancement scaling relation is compared with the one obtained by T05 in the lower left panel of Fig. 20. Our derived slope (0.47) falls between that found by T05 (0.28) and that of C06 (0.74) and agrees well with that derived by D05 (0.59). Our $[\alpha/\text{Fe}]$ ratio coincides with that of T05 at $\sigma_c = 250 \text{ km s}^{-1}$, while at $\sigma_c = 100 \text{ km s}^{-1}$ it is ~ 0.07 dex lower. The α -enhancement scaling relation is almost independent of the richness parameter, in very good agreement with C06 and T05.

As discussed in Sect. 3.9, there are no significant differences in the $[\alpha/\text{Fe}]$ ratios predicted by TMB03 and our models. Moreover, since C06 have also used the models presented here, we may exclude that the different slopes found by T05, C06, and us are due to the models. The only noticeable differences are in the data samples and in the adopted methods. In particular, the use of different index sets coupled with the different sensitivity of the indices to the enhancement may explain the significant variation of the slope found by different authors.

6.2. Gradients and galaxy formation

Besides global stellar population parameters and their relation with galaxy structural parameters, population gradients within galaxies give one of the most strongest constraints on galaxy formation. Spectrophotometric and chemical properties at various locations within a galaxy are in fact closely related to the process of galaxy formation and evolution. Numerical simulations of dissipative collapse of galaxies including star formation definitely predict strong radial gradients in chemical enrichment (Larson 1974a, 1975; Carlberg 1984). The predicted metallicity gradients are as steep as $\Delta \log Z / \Delta \log r \sim -0.35$ (Larson 1974a), ~ -1.0 (Larson 1975), and ~ -0.5 (Carlberg 1984). A further prediction of monolithic models is a steepening of the metallicity gradient with the potential well of the galaxy, which increases from about zero (in low mass galaxies) to ~ -0.5 in the most massive ones (Carlberg 1984; Bekki & Shioya 1999; Chiosi & Carraro 2002; Kawata & Gibson 2003; Kobayashi 2004).

On the contrary, the dissipationless collapse models predict no gradients in chemical enrichment (Gott 1973, 1975) and the occurrence of major mergers predicts a significant dilution (White 1980; Bekki & Shioya 1999). More recently, Kobayashi (2004) has simulated the formation and chemodynamical evolution of elliptical galaxies including radiative cooling, star formation, feedback from Type II and Ia supernovae and stellar winds, and chemical enrichment. Galaxies are supposed to form through the successive merging of galaxies with various masses, which varies between a major merger at one extreme and a monolithic collapse of a slow-rotating gas cloud at the other extreme. They predict an average metallicity gradient of $\Delta \log Z / \Delta \log r \sim -0.3 \pm 0.2$ and no correlation between metallicity gradients and mass. The variety of gradients stems from the difference in the merging histories; in line with previous findings, galaxies that form monotonically have steeper gradients, while galaxies that undergo major mergers have shallower gradients.

If metallicity gradients are more directly related to the degree at which star formation has reprocessed the gas inside the galaxy, $[\alpha/\text{Fe}]$ gradients give very strong constraints about the *duration* of the chemical enrichment process at different radii. According to Pipino & Matteucci (2004), an outside-in formation scenario would predict $[\text{Mg}/\text{Fe}]$ ratios increasing with galaxy radius (and

slightly older ages in the external regions compared to the central ones). On the other hand, an inside-out formation, as suggested to explain the abundance gradients in the Milky Way (e.g., Matteucci & Francois 1989), would produce a decrease of the [Mg/Fe] ratio with radius, since the outermost regions would evolve slower than the inner ones.

From an observational aspect, evidence of metallicity gradients comes from the increase of line-strength indices (Carollo et al. 1993; Davies et al. 1993; Saglia et al. 2000; Trager et al. 2000a; Mehlert et al. 2003; Wu et al. 2005) and the reddening of the colors (e.g., Peletier 1990) towards the center of early-type galaxies. However, there is not yet a clear picture of the radial gradient behavior with respect to velocity dispersion. Some authors have shown that elliptical galaxies with larger values of the central Mg₂ index tend to have steeper Mg₂ gradients (Gorgas, Efstathiou & Aragon-Salamanca 1990; Carollo, Danziger & Buson 1993; Gonzalez & Gorgas 1995). On the contrary, Kobayashi & Arimoto (1999) did not find any correlation between gradients and physical properties in the 80 early-type galaxies of their study. Along the same line are the studies of Proctor & Sansom (2002) and Mehlert et al. (2003). More recently, Forbes et al. (2005) have re-analyzed the data of Coma cluster ellipticals (Mehlert et al. 2003; Sanchez-Blasquez 2004) and have found evidence for the presence of stronger metallicity gradients in more massive ellipticals. The only significant gradient shown by our study is that of the metallicity, while age and α enhancement seem to be flat within $R_e/2$, though with a significant dispersion (Figs. 18 and 19). The average metallicity gradient is $\Delta \log Z / \Delta \log(r/r_e) \sim -0.21$. There is also evidence for a trend of the Z gradient with central velocity dispersion, in the sense that more massive galaxies tend to have shallower gradients (Fig. 19). We thus do not find evidence for a steepening of the metallicity gradient toward larger masses, even if we consider only galaxies in the relatively richer environment.

The flat distribution of α elements, on average, in spite of a well-established metallicity gradient, is a little intriguing. The latter suggests that stellar populations are not mixed within $r_e/2$ and that metal enrichment was more efficient in the central region than in the outskirts of the galaxies. An outside-in formation scenario predicts the existence of gradients in both metallicity and α enhancement, while merging would smear out stellar populations and dilute any gradient. Our observations indicate that the star formation proceeded on typical lifetimes not significantly different across $r_e/2$, but evidently with a larger efficiency in the center. It is easy to show, however, that the observed flat gradient in α enhancement is within the prediction of galaxy models. Using GALSYNTH², we have run a chemical evolution model with parameters suited for a typical massive early-type galaxy (briefly, high SFR for

a fraction of a Gyr and passive evolution thereafter) and we have obtained that the run of [Mg/Fe] between [Z/H]=0.5 and [Z/H]=0.5, where the majority of stars are formed, is well approximated by

$$[Mg/Fe] = 0.46 - 0.13 \times [Z/H], \quad (34)$$

Thus the expected gradient in [Mg/Fe] corresponding to $\Delta \log Z / \Delta \log(r/r_e) \sim -0.21$ is $\Delta [Mg/Fe] / \Delta \log(r/r_e) \sim 0.03$ in very good agreement with what was observed. To find full support for an outside-in formation scenario, more external regions should be observed and analyzed.

6.3. Rejuvenation

The lack of environmental effects on the metallicity- σ_c and $[\alpha/\text{Fe}]-\sigma_c$ relations suggests that *young* ages are not the result of a more prolonged star formation in the low density environment. Moreover, NGC 3136, NGC3607, NGC7135, and NGC 6776 are massive galaxies, metal rich and α -enhanced, for which simple stellar population fits provide ages of only a few Gyrs. If recently formed and on the short timescale suggested by their α -enhancement, these objects would appear like the very powerful ultra luminous infrared galaxies (ULIRGs) observed in the local universe. However, it is easy to show that their luminosity would exceed by at least one order of magnitude that of the local powerful ULIRGs. In fact, recent determinations of star formation timescales in these latter objects, by different methods, indicate that the gas content cannot sustain the observed luminosity for more than a few tens of Myr (e.g., Vega et al. 2005; Prouton et al. 2004). This implies SFR in excess of $10^4 \text{ M}_\odot/\text{yr}$ for the masses that correspond to the velocity dispersions of these galaxies and, consequently, bolometric luminosities that by far exceed the typical ones in the local ULIRGs.

All these considerations, together with the presence of morphology/kinematics signatures of recent interaction episodes in all the four quoted galaxies (see Appendix in Papers I and II), strongly support the idea that the young ages obtained are due to recent rejuvenation episodes of star formation and do not correspond to their epoch of formation. If so, what is the mass involved in the rejuvenation episode? It is difficult to answer this question because the fading of the indices (H β for example) in a composite population depends on the fraction of the young component and the epoch of the event. We can only proceed with a statistical argument, though we are aware that the number of galaxies is not large. Looking to the data of Fig. 14, we determine that about 15% of all the objects look rejuvenated. The threshold limit for rejuvenation is taken from the age limit of the higher density objects. Let us suppose that, since the average epoch of formation, *all* the galaxies underwent a single rejuvenation event with a probability that follows the halo merging rate, namely $\sim(1+z)^{3.2}$ (Le Fèvre et al. 2000). The average epoch of formation is taken from the line in Fig. 14 indicating an average age of about 8 Gyr.

² GALSYNTH is a web based interface for the chemo-spectrophotometric code GRASIL at <http://web.pd.astro.it/galsynth/index.php>

Assuming the above merging rate law, and a flat $\Omega_m=0.3$, $\Omega_\Lambda=0.7$, and $H_0 = 70 \text{ km sec}^{-1} \text{ Mpc}^{-1}$ Universe, we determine that 15% of the total merging events since a look back time of 8 Gyr occur within the last 2.2 Gyr. This time must correspond to the time during which the $H\beta$ index of a combined (old plus young) population remains above the selected threshold for rejuvenation and, of course, it will depend on the relative mass fractions of the old and young populations. Thus we have to seek for what fractional mass of the young component a combined population (8 Gyr plus the young component) maintains its $H\beta$ index above the threshold value, for a duration of about 2.2 Gyr.

After selecting a threshold value of $H\beta \sim 2.0$ (from the data in Fig. 14), we find that the mass fraction of such a young population is $\sim 25\%$ of the total mass. We conclude that the data of Fig. 14 are compatible with *all* galaxies having undergone a merger event since their formation, where not more than 25% of their total mass has been converted into stars. For a larger mass fraction, the fraction of rejuvenated objects we would see today would be larger. In other words, 75% of the total mass is definitely old, even if the galaxies suffered a major merger in their life.

7. Summary and conclusions

We have analyzed the stellar populations of the sample of 65 early-type galaxies mainly located in the field, presented in Papers I and II. Our sample is biased towards early-type galaxies selected on the basis of ISM traces, in particular optical emission lines, tracing the warm ISM component. On the other hand, considering the incidence of galaxies showing a warm ISM in a randomly selected sample of early-type galaxies quoted by Falcon-Barroso et al. (2006), i.e., 75 %, (83% in the field), we are confident that our sample is not very dissimilar from those with which we compare our results.

Stellar population parameters age, metallicity, and $[\alpha/\text{Fe}]$ ratio have been derived for all the apertures and gradients of the sample by the comparison of the Lick indices with new SSP models, presented in this work, which account for the presence of non-solar element abundance patterns. New SSP models have been developed for a wide range of ages ($10^9 - 16 \times 10^9 \text{ yr}$), metallicities ($Z=0.0004, 0.004, 0.008, 0.02, 0.05$), and $[\alpha/\text{Fe}]$ ratios (0-0.8). The SSPs are based on the Padova stellar evolution tracks and accompanying isochrones (Bertelli et al. 1994; Bressan et al. 1994), which have been previously calibrated on color-magnitude diagrams of several star clusters in the Galaxy and in the Magellanic Clouds.

The standard composition line-strength indices are computed on the basis of the fitting functions of Worthey et al. (1994) and Worthey & Ottaviani (1997). The enhanced SSPs are computed by applying an index correction, which we derive following the main guidelines provided by previous works in the literature (TMB03, Tantalo & Chiosi 2004a), although with revised index dependence

on the element abundance, to the standard SSPs. More specifically, we find that a logarithmic dependence of the index with element abundance provides a more satisfactory description of the index behavior. This evidence is also supported by preliminary results obtained running new model atmospheres and synthetic spectra with the code ATLAS12, that consistently computes both interior and emergent spectra models with arbitrary abundances. The correction for the effects of α -enhancement is computed on the basis of the most recent specific index responses computed by Korn et al. (2005) for different metallicities.

The new α -enhanced SSPs have been implemented within an algorithm devised to derive stellar population parameters from the observed line-strength indices. The method, which rests on the probability density function, provides, together with the most probable solution in the (age, Z , $[\alpha/\text{Fe}]$) space, the solutions along the age-metallicity degeneracy that are within 1σ error from the observed index values.

Summarizing our results:

- The derived age distribution shows a wide spread, with SSP-equivalent ages from a few Gyr to 15 Gyr and with lenticular galaxies being generally younger than ellipticals (the average ages for the whole sample, E and S0 are 8, 8.7, and 6.3 Gyr, respectively); the metallicity distribution shows a broad peak at $0 < [Z/H] < 0.3$; finally, the $[\alpha/\text{Fe}]$ ratio definitely presents a peak at ~ 0.22 , with a narrower distribution than for age and metallicity.

We also seek possible correlation of the stellar population parameters with both central velocity dispersion and local galaxy density.

- Concerning the relation with the galaxy potential well, we do not find the clear signature of a global trend of age with velocity dispersion; on the other hand, significant positive trends are derived for metallicity and α/Fe enhancement.
- The robust metallicity- σ_c relation testifies that chemical enrichment is more efficient in more massive galaxies and, within a universal initial mass function, the relation between the α/Fe enhancement and the velocity dispersion indicates that the overall duration of the star formation process is shorter within deeper potential wells. These two relations do not depend on galaxy morphological type, unlike the age- σ_c relation, indicating that the galaxy gravitational potential is the main driver of the chemical enrichment process of the galaxy.

We analyzed the relations of the stellar population parameters with the local galaxy density ρ_{xyz} and we obtained the following results:

- Concerning the age- ρ_{xyz} relation, we derive a clear dichotomy: while very young objects (from 1 Gyr to 4

Gyr, some of which have high σ_c) are found in very low density environments ($\rho_{xyz} \leq 0.4$), none of the galaxies in high density regions (40 % of the sample with measured density) is younger than 4-5 Gyr. No trend of the chemical enrichment path is found with environmental conditions. The lack of environmental effect on the (α -enhancement)- σ_c relation indicates that in very low environments rejuvenation episodes, rather than more prolonged star formation, are frequent.

We analyzed the stellar population gradients within the single galaxies:

- We definitely derive negative metallicity gradients (metallicity decreases from the central regions outwards) of the order of $\Delta \log Z / \Delta \log(r/r_e) \sim -0.21$, consistently with literature values. On average the α -enhancement remains quite flat within $r_e/2$, but this is consistent with the observed metallicity gradient. The only strong correlation is that of the metallicity gradient with velocity dispersion: larger negative gradients are derived for less massive systems and become shallower at increasing galaxy mass.

From the above results, we try to sketch a possible scenario for galaxy formation. The potential well of the galaxy seems to be the main driver of the chemical path during its formation, with more massive galaxies exhibiting the more efficient chemical enrichment and shorter star formation timescale. Furthermore, galaxies in denser environments are on average older than galaxies in less dense environments. This is in agreement with recent models of galaxy formation that combine feedback from QSO and SN, and cooling of the gas (Granato et al. 2001, 2004).

Galaxies in less dense environments also show signatures of very recent rejuvenation episodes. By comparing the number of “young” objects with the total number of galaxies, and by means of simple two-SSP component models, we estimate that in these rejuvenation episodes (like major mergers), not more than 25% of the galaxy mass could be formed. Thus we estimate that, even if spheroidal galaxies are affected by major mergers during their evolution, about 75% of the galaxy mass is formed during the initial epoch of formation.

Acknowledgements. The authors would like to thank the referee, Dr. H. Kuntschner, whose comments and suggestions significantly contributed to improve the paper. We acknowledge P. Bonifacio and F. Castelli for having kindly provided us with the ATLS12 code and for their contribution in the computation of model atmospheres. RR and WWZ acknowledge the partial support of the Austrian and Italian Foreign Offices in the framework of the science and technology bilateral collaboration (project number 25/2004). WWZ acknowledges the partial support of the Austrian Science Fund (project P14783) and of the Bundesministerium für Bildung, Wissenschaft und Kultur. AB acknowledges warm hospitality by INAOE (Mex).

References

Annibali, F. 2005, Ph.D. Thesis, SISSA/ISAS, Trieste

Annibali, F., Bressan, A., Rampazzo, R., Zeilinger, W.W. 2005, AA, in press (astro-ph/0508520): PaperII

Arimoto, N., & Yoshii, Y. 1987, A&A, 173, 23

Baugh, C. M., Cole, S., & Frenk, C. S. 1996, MNRAS, 283, 1361

Bekki, K., & Shioya, Y. 1999, ApJ, 513, 108

Bender, R., Paquet, A. 1995, IAU Symp. 164: Stellar Populations, 164, 259

Bertelli, G., Bressan, A., Chiosi, C., Fagotto, F., Nasi, E. 1994, AAS 106, 275

Beuing, J., Bender, R., Mendes de Oliveira, C., Thomas, D., Maraston, C. 2002, AA 395, 431

Blum, R. D. 1995, ApJL, 444, L89

Bressan, A., Chiosi, C., Fagotto, F. 1994, ApJS 94, 63

Bressan, A., Chiosi, C., Tantalo, R. 1996, AA 311, 425

Bruzual, G., & Charlot, S. 2003, MNRAS, 344, 1000

Buzzoni, A., Gariboldi, G., Mantegazza, L. 1992, AJ 103, 1814

Buzzoni, A., Mantegazza, L., Gariboldi, G. 1994, AJ 107, 513

Carlberg, R. G. 1984, ApJ, 286, 403

Carollo, M., Danziger, I.J., Buson, L.M. 1993, MNRAS 265, 553

Carollo, M., Danziger, I.J. 1994, MNRAS 270, 523

Chavez, M., Malagnini, M. L., & Morossi, C. 1996, ApJ, 471, 726

Chiosi, C., & Carraro, G. 2002, MNRAS, 335, 335

Clemens, M. S., Bressan, A., Nikolic, B., Alexander, P., Annibali, F., & Rampazzo, R. 2006, MNRAS, 370, 702

Conti, P. S., Deutsch, A. J. 1967, ApJ 147, 368

Castelli, F., Kurucz, R. L. 2003, IAU Symposium, 210, 20P

Davies, R. L., Sadler, E. M., Peletier, R. F. 1993, MNRAS 262, 650

Denicoló, G., Terlevich, R., Terlevich, E., Forbes, D. A., Terlevich, A., & Carrasco, L. 2005a, MNRAS, 356, 1440

Denicoló, G., Terlevich, R., Terlevich, E., Forbes, D. A., & Terlevich, A. 2005b, MNRAS, 358, 813: D05

De Vaucouleurs, G., de Vaucouleurs, A., Corwin, H.G. Jr. et al. 1991 *Third Reference Catalogue of Bright Galaxies*, Springer-Verlag, New York

Edvardsson, B., Andersen, J., Gustafsson, B., Lambert, D. L., Nissen, P. E., & Tomkin, J. 1993, A&AS, 102, 603

Falcón-Barroso, J., Sarzi, M., Bacon, R. et al. 2006, New Astron. Reviews, 49, 515

Fisher, D., Franx, M., Illingworth, G. 1995, ApJ 448, 119

Forbes, D. A., Sánchez-Blázquez, P., & Proctor, R. 2005, MNRAS, 361, L6

Fuhrmann, K. 1998, A&A, 338, 161

Gabel, J. R., Bruhweiler, F. C., Crenshaw, D. M., Kraemer, S. B., & Miskey, C. L. 2000, ApJ, 532, 883

Gallazzi, A., Charlot, S., Brinchmann, J., White, S. D. M., & Tremonti, C. A. 2005, MNRAS, 362, 41: G05

Girardi, L., Bressan, A., Bertelli, G., & Chiosi, C. 2000, A&A, 141, 371

Gonzalez, J.J. 1993, Ph.D. thesis, Univ. California, Santa Cruz: G93

Gonzalez, J. J., & Gorgas, J. 1995, ASP Conf. Ser. 86: Fresh Views of Elliptical Galaxies, 86, 225

Gorgas, J., Efstathiou, G., & Salamanca, A. A. 1990, MNRAS, 245, 217

Gott, R. J. 1973, ApJ, 186, 481

Gott, J. R. 1975, IAU Symp. 69: Dynamics of the Solar Systems, 69, 271

Goudfrooij, P. 1998, in *Star Formation in Early-Type Galaxies*, ASP Conference Series 163, ed.s P. Carral and J. Cepa, 55

Granato, G. L., Silva, L., Monaco, P., Panuzzo, P., Salucci, P., De Zotti, G., & Danese, L. 2001, MNRAS, 324, 757

Granato, G. L., De Zotti, G., Silva, L., Bressan, A., & Danese, L. 2004, ApJ, 600, 580

Greggio, L., Renzini, A. 1983, AA 118, 217

Grevesse, N., & Sauval, A. J. 1998, Space Science Reviews, 85, 161

Ho, L.C., Filippenko A.V., Sargent W.L.W. 1997, ApJ 112, 31

Kauffmann, G., White, S. D. M., & Guiderdoni, B. 1993, MNRAS, 264, 201

Kawata, D., & Gibson, B. K. 2003, MNRAS, 346, 135

Kobayashi, C., & Arimoto, N. 1999, ApJ, 527, 573

Kobayashi, C. 2004, MNRAS, 347, 740

Korn, A. J., Maraston, C., & Thomas, D. 2005, A&A, 438, 685: K05

Kuntschner, H. 2000, MNRAS 315, 184

Kuntschner, H., Smith, R.J., Colless, M. et al. 2002, MNRAS 337, 172

Kurucz, R. L. 1993b, ASP Conf. Ser. 44: IAU Colloq. 138: Peculiar versus Normal Phenomena in A-type and Related Stars, 44, 87

Jørgensen, I. 1999, MNRAS 306, 607

Larson, R. B. 1974a, MNRAS, 166, 585

Larson, R. B. 1974b, MNRAS, 169, 229

Larson, R. B. 1975, MNRAS, 173, 671

Le Fèvre, O., et al. 2000, MNRAS, 311, 565

Leonardi, A.J., Rose, J.A. 1996, AJ 111, 182

Longhetti, M., Rampazzo, R., Bressan, A., Chiosi, C. 1998, AA 130, 251

Longhetti, M., Bressan, A., Chiosi, C., Rampazzo, R. 1999, AA 345, 419

Longhetti, M., Bressan, A., Chiosi, C., Rampazzo, R. 2000, AA 353, 917

Macchetto, F., Pastoriza, M., Caon, N., Sparks, W.B., Giavalisco, M. et al. 1996, AAS 120, 463

Matteucci, F., Greggio, L. 1986, AA 154, 279

Matteucci, F., & Francois, P. 1989, MNRAS, 239, 885

McWilliam, A., & Rich, R. M. 1994, ApJS, 91, 749

Mehlert, D., Saglia, R. P., Bender, R., Wegner, G. 1998, AA 332, 33

Mehlert, D., Saglia, R. P., Bender, R., & Wegner, G. 2000, A&AS, 141, 449

Mehlert, D., Thomas, D., Saglia, R.P., Bender, R., Wegner, G. 2003, AA 407, 423

Michard, R., & Marchal, J. 1994, A&A, 105, 481

Morganti, R., Sadler, E. M., Oosterloo, T. A., Pizzella, A., & Bertola, F. 1997, Publications of the Astronomical Society of Australia, 14, 89

Munari, U., Sordo, R., Castelli, F., Zwitter, T., 2005, MNRAS, astro-ph/0502047: Mu05.

Nomoto, K., Thielemann, F.-K., & Wheeler, J. C. 1984, ApJL, 279, L23

Osterbrock, D., 1989, in *Astrophysics of Planetary Nebulae and Active Galactic Nuclei*, University Science Books

Pagel, B. E. J., Tautvaisiene, G. 1995, MNRAS 276, 50S

Peletier, R. F. 1989, Ph.D. Thesis

Peletier, R. F. 1990, ASP Conf. Ser. 14: Astrophysics with Infrared Arrays, 14, 32

Pipino, A., & Matteucci, F. 2004, MNRAS, 347, 968

Proctor, R. N., & Sansom, A. E. 2002, MNRAS, 333, 517

Prouton, O. R., Bressan, A., Clemens, M., Franceschini, A., Granato, G. L., & Silva, L. 2004, A&A, 421, 115

Puzia, T.H., Saglia, R.P., Kissler-Patig, M., Maraston, C., Greggio, L. et al. 2002, AA 395, 45

Ramírez, S. V., Stephens, A. W., Frogel, J. A., & DePoy, D. L. 2000, AJ, 120, 833

Rampazzo R., Annibali F., Bressan A., Longhetti M., Padoan F., Zeilinger W.W. 2005, AA 433, 497: PaperI

Saglia, R. P., Maraston, C., Greggio, L., Bender, R., & Ziegler, B. 2000, A&A, 360, 911

Salaris, M., & Weiss, A. 1998, A&A, 335, 943

Salasnich, B., Girardi, L., Weiss, A., & Chiosi, C. 2000, A&A, 361, 1023

Salpeter, E. E. 1955, ApJ 121, 161

Sanchez-Blazquez, P. 2004, Ph.D. Thesis

Sandage, A.R., Tamman, G. 1987, *A Revised Shapley Ames Catalogue of Bright Galaxies*, Carnegie, Washington (RSA)

Sarzi, M., Falcón-Barroso, J., Davies, R.L., Bacon, R. et al. 2006, MNRAS, 366, 1151

Steinmetz, M., & Navarro, J. F. 2002, New Astronomy, 7, 155

Tantalo, R., Chiosi, C., Bressan, A., Fagotto, F. 1996, AA 311, 361

Tantalo, R., Chiosi, C., & Bressan, A. 1998, AA 333, 419

Tantalo, R., & Chiosi, C. 2004a, MNRAS, 353, 917

Tantalo, R., & Chiosi, C. 2004b, MNRAS, 353, 405

Tantalo, R., Chiosi, C., Munari, U., Piovan, L. & Sordo, R., astro-ph/0406314

Thielemann, F.-K., Nomoto, K., & Hashimoto, M.-A. 1996, ApJ, 460, 408

Thomas, D., Greggio, L., Bender, R. 1998, MNRAS 296, 119

Thomas, D., & Maraston, C. 2003, A&A, 401, 429

Thomas, D., Maraston, C., Bender, R. 2003, MNRAS 339,897: TMB03

Thomas, D., Maraston, C., Korn, A. 2004, MNRAS 351, L19

Thomas, D., Maraston, C., Bender, R. 2005, ApJ 621, 673: T05

Toomre, A. 1977, Evolution of Galaxies and Stellar Populations, 401

Trager, S.C., Worthey, G., Faber, S.M., Burstein, D., Gozalez J.J. 1998, ApJS 116, 1

Trager, S.C., Faber, S.M., Worthey, G., Gozalez J.J. 2000a, AJ 119, 164

Tripicco, M. J., Bell, R. A. 1995, AJ 110, 3035

Tully, R.B. 1988, *Nearby Galaxy Catalogue*, Cambridge University Press

VandenBerg, D. A., Swenson, F. J., Rogers, F. J., Iglesias, C. A., & Alexander, D. R. 2000, ApJ, 532, 430

van Dokkum, P. G., & Franx, M. 1995, AJ, 110, 2027

Varnas, S. R., Bertola, F., Galletta, G., Freeman, K. C., & Carter, D. 1987, ApJ, 313, 69

Vazdekis A. 1999, ApJ 513, 224

Weiss, A., Peletier, R. F., & Matteucci, F. 1995, A&A, 296, 73

Vega, O., Silva, L., Panuzzo, P., Bressan, A., Granato, G. L., & Chavez, M. 2005, MNRAS, 364, 1286

White, S. D. M. 1980, MNRAS, 191, 1P

Woosley, S. E., & Weaver, T. A. 1995, ApJS, 101, 181

Worthey, G. 1992, Ph.D. Thesis, University of California, Santa Cruz

Worthey, G., Faber, S. M., Gonzalez, J. J. 1992, ApJ 398, 69

Worthey, G. 1994, ApJS, 95, 107

Worthey, G., Faber, S.M., Gonzalez, J.J., Burstein, D. 1994, ApJS 94, 687

Worthey, G., Ottaviani, D.L. 1997, ApJS 111, 377

Wu, H., Shao, Z., Mo, H. J., Xia, X., & Deng, Z. 2005, ApJ, 622, 244